Title
K* AND N* PRODUCTION BY 1.96-BeV/c K+ MESONS INTERACTING WITH HYDROGEN

Author
O'Halloran, Thomas Alphonsus

Publication Date
1963-10-16

UCRL-11068

University of California

Ernest O. Lawrence Radiation Laboratory

K^* AND N^* PRODUCTION BY 1.96-BeV/c K^+ MESONS INTERACTING WITH HYDROGEN

Berkeley, California

DISCLAIMER

Research and Development

UCRL-11068
UC-34 Physics
TID-4500 (19th Ed.)

UNIVERSITY OF CALIFORNIA
Lawrence Radiation Laboratory
Berkeley, California

AEC Contract No. W-7405-eng-48

K^* AND N^* PRODUCTION BY 1.96-BeV/c K^+ MESONS INTERACTING WITH HYDROGEN

Thomas Alphonsus O'Halloran, Jr.

(Thesis)

October 16, 1963

K^* AND N^* PRODUCTION BY 1.96-BeV/c K^+ MESONS INTERACTING WITH HYDROGEN

Contents

K^* AND N^* PRODUCTION BY 1.96 BeV/c K^+ MESONS INTERACTING WITH HYDROGEN

Thomas Alphonsus O'Halloran, Jr.

Lawrence Radiation Laboratory
University of California
Berkeley, California

October 16, 1963

ABSTRACT

The Brookhaven National Laboratory's 20-inch hydrogen bubble chamber was exposed to a separated K^+-meson beam. Cross sections for the inelastic processes at 1.96 BeV/c are measured. The inelastic processes are dominated by the production of two resonances, the I = 1/2 K-π resonance (K^*), and the I = 3/2 pion-nucleon resonance (N^*).

The four-particle state is dominated by the simultaneous production of these two resonances. Experimental evidence is presented which indicates that the one-pion exchange dominates this reaction for momentum transfers as high as 25 m_π^2. We can calculate the observed cross section by including a form factor in the one-pion-exchange calculations.

The three-particle state is also dominated by the production of either the K^* of N^*. Production of the N^* cannot proceed via the one-pion exchange. Experimental evidence is presented which indicates that this process proceeds via the exchange of a vector meson.

I. INTRODUCTION

One of the first results of the early $\bar{p}$-p annihilation studies was that the average pion multiplicity exceeded the predictions of the statistical model. It was then conjectured that one way in which the pion multiplicity could be reconciled to the statistical model was by the existence of π-π resonances which could reduce the observed multiplicity.[1] At the same time it was also speculated that the form factors observed in the electron-scattering experiments were likewise the result of π-π resonances.[2] Thus, in 1960 several research groups made a determined effort to discover the π-π resonances in the pion spectrum of the $\bar{p}$-p annihilations and in the pion spectrum produced by inelastic pion interactions.

In a period of three years, resonances have been discovered not only between pions, but also between all known strongly interacting particles. Thus the list of elementary particles has been extended from ten particles to include 45 resonant states of various charge, spin, and strangeness.[3] The measurement of the quantum numbers of these resonances and the search for additional resonances accounts for a major portion of current research in elementary-particle physics.

Along with the discovery of the resonant states some progress has also been made in the study of the dynamics of the production of these states. One of the most interesting is the peripheral model, in which the reaction is considered to be dominated by the exchange of the least massive particle between the colliding particles, subject to the conservation laws of strong interactions.[4] It might be expected that the inelastic processes which produce the resonances in the final state would not behave in the same manner as elastic scattering. The least massive strongly interacting particle is the pion. For elastic meson scattering, however, the one-pion exchange is forbidden by parity and angular-momentum considerations at the pion vertex. For elastic nucleon and antinucleon scattering, the pseudoscalar coupling of the pion to the nucleon requires the one-pion-exchange contribution

to vanish in the forward direction. Thus, if the one-pion exchange is to play a dominant role in any physical process, it is the inelastic processes to which one must look.

In this dissertation we discuss mainly the inelastic processes leading to the production of two resonances, the K^* and the N^*. The reactions we consider were produced by 1.96-BeV/c K^+ mesons interacting with hydrogen in the 20-inch Brookhaven National Laboratory bubble chamber. The resonances are observed in reactions leading to single pion production and double pion production.

Earlier results of this experiment have enabled us to show that the four-body final state is dominated by the production of a double-resonant final state and also to determine the spin of the K^* to be 1.[5] We now use the observed alignment in the angle between the incoming K^+ and the outgoing K^+ in the K^* rest frame as an analyzer to investigate the dynamics of the reaction. We find that the reaction can be described by the one-pion-exchange model. To fit the data, however, we must introduce into the theoretical model a form factor dependent upon momentum transfer.

The three-body final states do not appear to be as simple as the four-body final states. We find no evidence for the same alignment in the K^* rest frame as we observed in the four-body final states. In the three-body final state, the N^* cannot be produced by the one-pion exchange because of angular-momentum and parity considerations at the $KK\pi$ vertex. For these events we find evidence for the exchange of a vector meson.

In section II we discuss the experimental arrangement and procedures used for the scanning, measurement, and analysis of the events. In section III we discuss the analysis of the data to obtain the partial cross sections and the analysis of the final states for the three-body and four-body final states. Finally, in section IV we calculate the cross sections by using the one-pion-exchange model as formulated by the Salzmans.[6]

Our results on the meson exchange in the reaction $K^+ + p \rightarrow K^* + N^*$ and on the vector-meson exchange in the reaction $K^+ + p \rightarrow K^0 + N^*$ have been reported in the literature.[7,8]

II. EXPERIMENTAL PROCEDURES AND DATA ANALYSIS

A. Beam Design

The experiment was carried out with the 20-inch hydrogen bubble chamber at Brookhaven National Laboratory in the Brookhaven-Yale beam of the alternating-gradient synchrotron (AGS). The beam layout and design have been described in the literature,[9] and we shall give only a brief description of the beam and the procedure used to retune the beam to the desired momentum.

The beam is shown schematically in Fig. 1. The first stage, the transport section, has two primary functions. It demagnifies the target, focusing the image on slit 2, which serves as a source for the remaining part of the beam, and also gives a rough momentum determination for the beam. The next two stages consist of velocity spectrometers BS1 and BS2, and the associated quadrupole optics. Slit 3 serves as a mass-resolution slit at the end of the first separation stage. At the beginning of the second separation stage, precise momentum definition is obtained by virtue of a large-angle deflection of the beam. The fourth slit serves as a momentum-defining and mass-resolution slit. The final stage is a beam-shaping section to shape the image to fill the chamber.

The beam was tuned by means of counters near the final mass slit. The system was tuned by setting the magnetic field of the first velocity spectrometer and then varying the field of the second velocity spectrometer. The second spectrometer is used as an analyzer, and by taking counting rates as a function of the field of the second spectrometer, one can study the image width and the separation of the beam. Figure 2 shows the steps in the tuning procedure. In Fig. 2a we have peaked spectrometer 1 to transmit pions. In Fig. 2b we have increased the field in BS1; as a result the pion transmission is decreased and the kaon transmission begins to appear as a shoulder on the pion peak. Figure 2c shows the operating conditions. From the tuning curves, we estimate the pion contamination to be less than 3%.

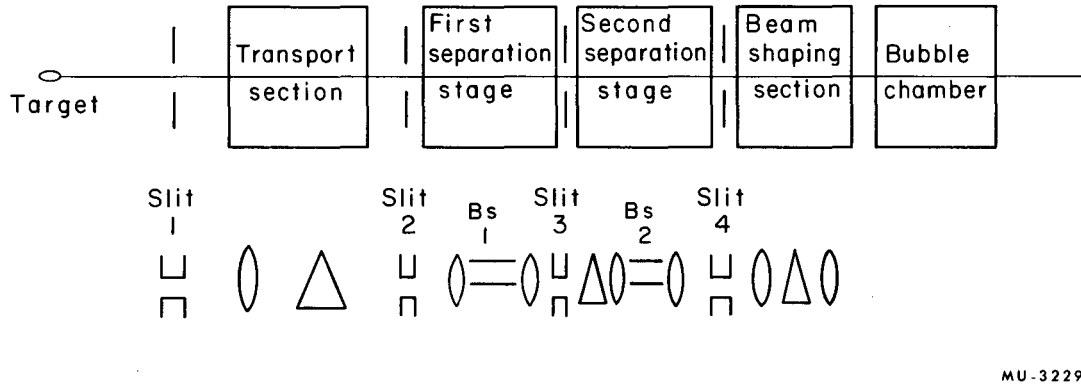

Fig. 1. Schematic diagram of the beam.

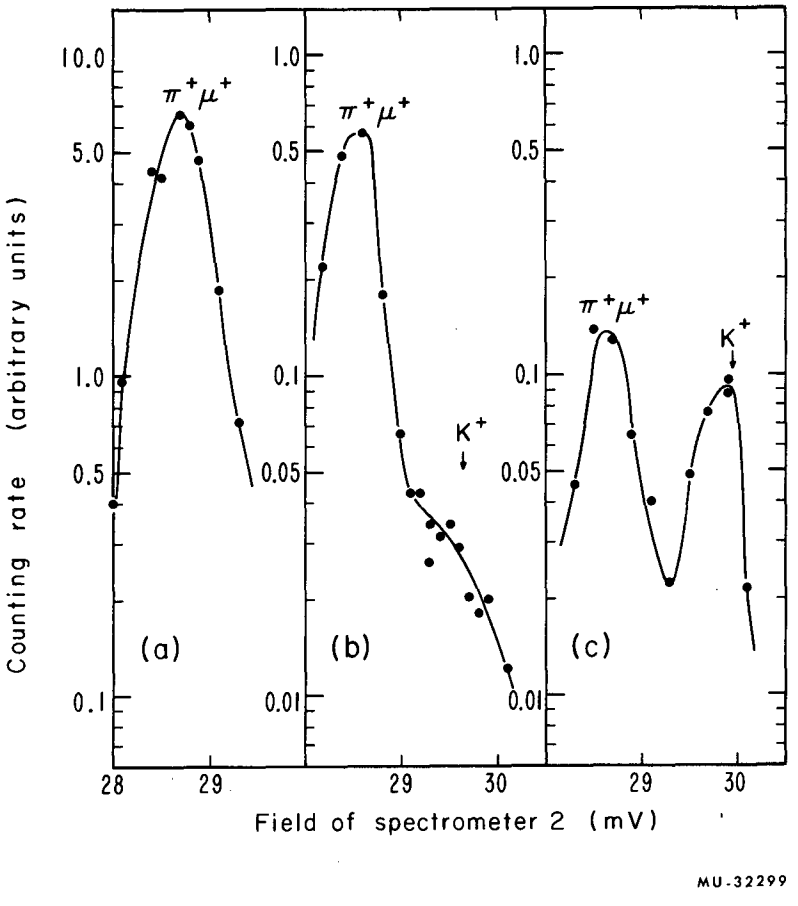

Fig. 2. Tuning curves at 1.96 BeV/c. (a) Peaked on pions. (b) Intermediate step in the tuning. (c) Running conditions.

B. Scanning and Measurement

A total of 20 000 frames was exposed to a 1.96-BeV/c separated K^+ beam. It was found that by scanning the film twice we could achieve essentially 100% efficiency for the various final states. All tracks that interacted were then sketched and classified topologically. When it was desired to examine a selected topological event type, the sketch cards were selected and the events were measured on a digitized measurement machine (the Franckenstein), which punched the projected x and y coordinates for each track of an event on an IBM card. By measuring each track in two stereoscopic views, we could spatially reconstruct the track on an IBM 7090 computer, and each track momentum could be obtained from the curvature measurements.[10]

The events were constrained to lie within a selected fiducial volume in the center of the chamber 38 cm long and 14 cm wide, and were then subjected to a kinematical analysis by the least-squares kinematical fitting routine GUTS, which is the main part of the program KICK. An attempt was made to fit all possible configurations in the final state as each track was given all possible interpretations. The output was then examined by a physicist at the scanning table. To be accepted, an event had to satisfy two criteria. Its χ^2 value had to be within predetermined limits ($\gtrsim$ 1% confidence limit), and the observed ionization had to be consistent with the fitted momentum and mass assignment for each track.

The χ^2 distributions for the reactions $K^+ + p \rightarrow K^0 + \pi^+ + p$ and $K^+ + p \rightarrow K^+ + \pi^- + \pi^+ + p$ are given in Fig. 3. For the three-particle final state, we have used only K^0's that decay via the two-charged-pion decay mode and have been fitted by KICK at the decay vertex. Both curves, therefore, are four-constraint fits, and the mean value of the χ^2 should be four. The average χ^2 values are 6 for the four-body final state and 4.9 for the three-body final state. This indicates that the errors were underestimated by 22.5% and 10.7% for the four-body and three-body final states, respectively. The curves in Fig. 3 are for a theoretical χ^2 distribution which has been calculated with a scale factor of $[1/1.225]^2$ and $[1/1.107]^2$ for the four-body and three-body final states, respectively.

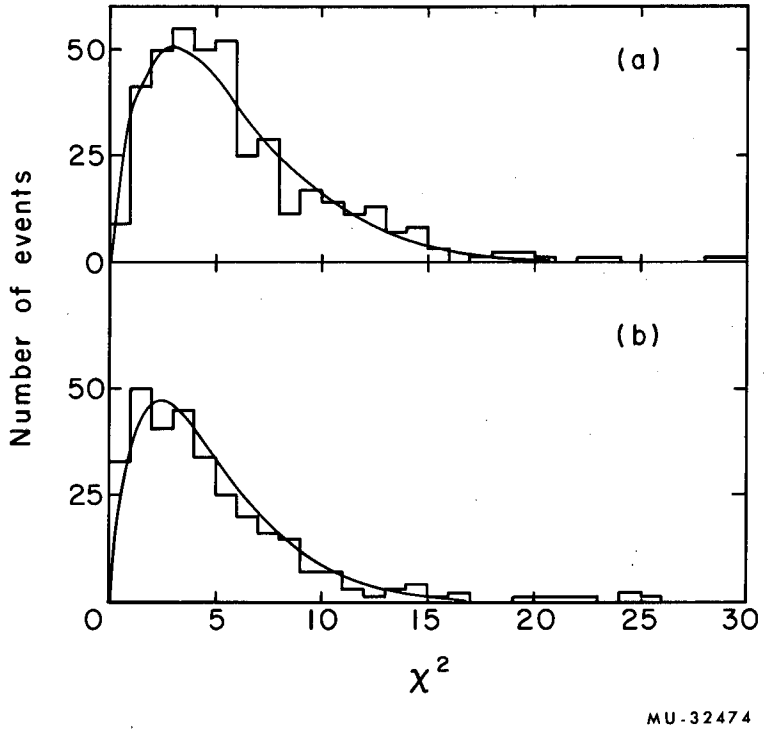

Fig. 3. Chi-square distributions for three-body and four-body final states. The number of constraints in each case is four. Curve (a) is for the reaction $K^+ + p \rightarrow K^+ + \pi^- + \pi^+ + p$, with $\langle \chi^2 \rangle = 6.0$. Curve (b) is for the reaction $K^+ + p \rightarrow K^0 + \pi^+ + p$, with $\langle \chi^2 \rangle = 4.9$.

We have also used the three-body final state to obtain an estimate of the resolution of the experiment. To do this, we have deleted any information on the K^0 and fitted the decay pions at the production vertex. This gives a four-constraint fit. We have then calculated the invariant mass of the decay pions. The mean weighted value is 499.0 ± 0.2 MeV. The error quoted is statistical only. We then proceeded to delete the π^- from the fitting procedure. The fit in this case is for one constraint. The mean weighted value for the one-constraint fits is 498.0 ± 0.5 MeV. Again the quoted error is statistical only. In Fig. 4 we show the mass distributions. The curves are fitted Gaussian curves. The central mass for the fitted Gaussian is found to be 498.5 MeV for the four-constraint fits and 500.7 MeV for the one-constraint fits. The full width at half maximum is 7.4 MeV for the four-constraint fits and 21.8 MeV for the one-constraint fits.

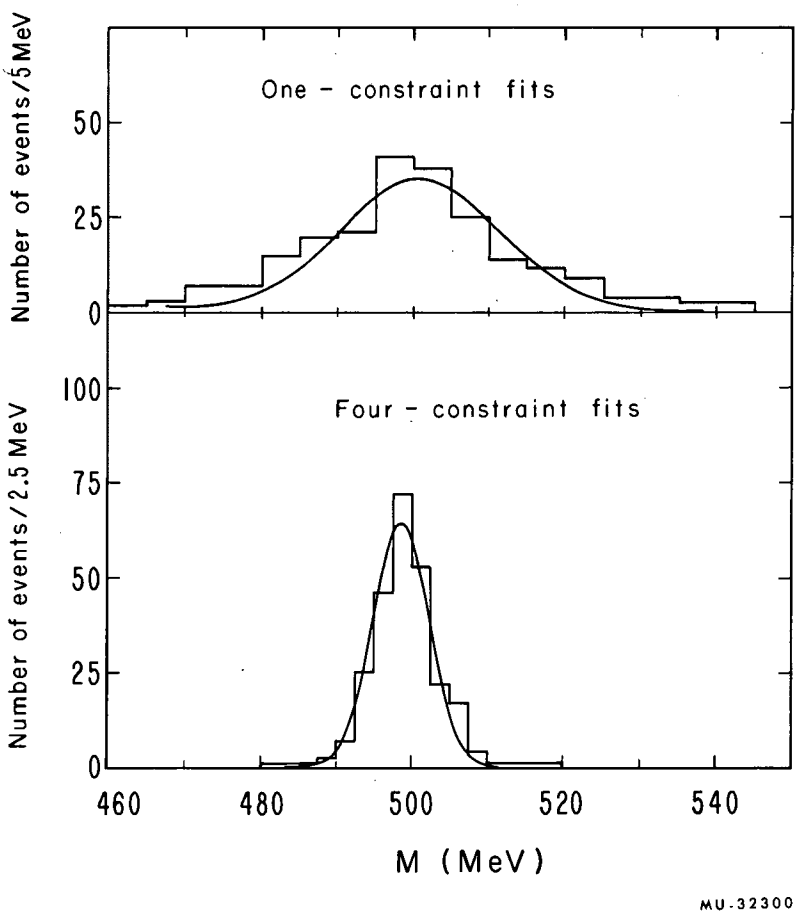

Fig. 4. Invariant mass of the pions from K_1^0 decay fitted to the production vertex. For one-constraint fits, the full width at half maximum is 21.8 MeV. For the four-constraint fits the full width at half maximum is 7.4 MeV.

III. EXPERIMENTAL RESULTS

A. Experimental Cross Sections

The total beam path length in the bubble chamber was determined from the number of "τ-like" decays. A τ-like decay is defined as a decay that has three charged particles in the final state (i.e., τ mesons and K^+ decays with Dalitz pairs). The branching ratio for this mode of decay is 0.061.[11] The path length can be determined from the relation

$$L = \frac{1}{f} \frac{cp}{M} c\,t\,N,$$

where f is the "τ-like" decay branching ratio, p is the beam momentum in BeV/c, M is the K^+-meson mass in BeV, t is the K^+-meson lifetime, and N is the number of observed τ-like decays. We observe 290 decays and find a total path length of $6.9 \pm 0.4 \times 10^6$ cm. This is equivalent to a cross section of 3.88 μb/event.[12]

The manner of determining the total number of events varied with the topology of the final state. To discuss this, we define three classes of events:

(a) events with four charged particles in the final state,

(b) events with two charged particles in the final state which are accompanied by the decay of a neutral V^0,

(c) events with only two charged particles in the final state.

Events in class (a) are the result of a complete double scan and analysis of the film. Each event has been examined by a physicist, and the results of the kinematical fitting are consistent with the ionization observed on the scan table.

Events in class (b) are also the result of a complete double scan and analysis of the film. The neutral V^0 was first fitted to the decay modes $K^0 \rightarrow \pi^+ + \pi^-$ and $\Lambda^0 \rightarrow \pi^- + p$. No events were found which fit the lambda decay mode. As a result, we can set an upper limit on the cross section for the reaction $K^+ + p \rightarrow K^+ + K^+ + \Lambda^0$. The dominating final state was found to be $K^0\pi^+p$, and we have used the K_1^0 mode of decay into two charged pions to obtain the total cross sections.

To use the K_1^0 mode of decay into two charged pions to calculate the cross section, we must introduce two corrections:

1. A correction for the fact that only 1/3 of all K^0 mesons decay via charged pions in the K_1^0 mode. To obtain the total number of K^0 mesons produced, the observed sample must be multiplied by a factor of 3.

2. A geometric correction. We must consider the probability that the K_1^0 may not decay in the chamber, the chamber being of finite dimensions. This probability depends on the momentum P of the K_1^0 and the potential path length of the K_1^0 from its production vertex to the limits of the fiducial volume along its flight path L. The proper time that the K_1^0 spends in the bubble chamber is

$$T = \frac{M_{K_1^0}}{Pc} \frac{L}{c} ,$$

and the probability that it will decay inside the fiducial volume is

$$P_D = 1 - e^{-T/T_0},$$

where $T_0 = 0.88 \times 10^{-10}$ sec is the K_1^0 lifetime.[13] Each event was divided by this probability. All distributions were examined with and without this weighting factor. No correlation between the weighting factor and any physical variable was noted. The average correction was 15%. In Fig. 5 we show the lifetime distribution for the corrected number of events.

Events in class (c) are the result of a double scan of the film, but have been only partially analyzed. Events in this category can be either elastic, which can be kinematically fitted with four constraints, or inelastic, which must be kinematically fitted with only one constraint. Since the one-constraint fits usually give ambiguities in the fitted events, we must rely on the ionization to distinguish the final states. To do this we have selected several rolls of film in which the ionization appears to be "ideal." To a large extent this is based on the experience gained in analyzing the events in classes (a) and (b).

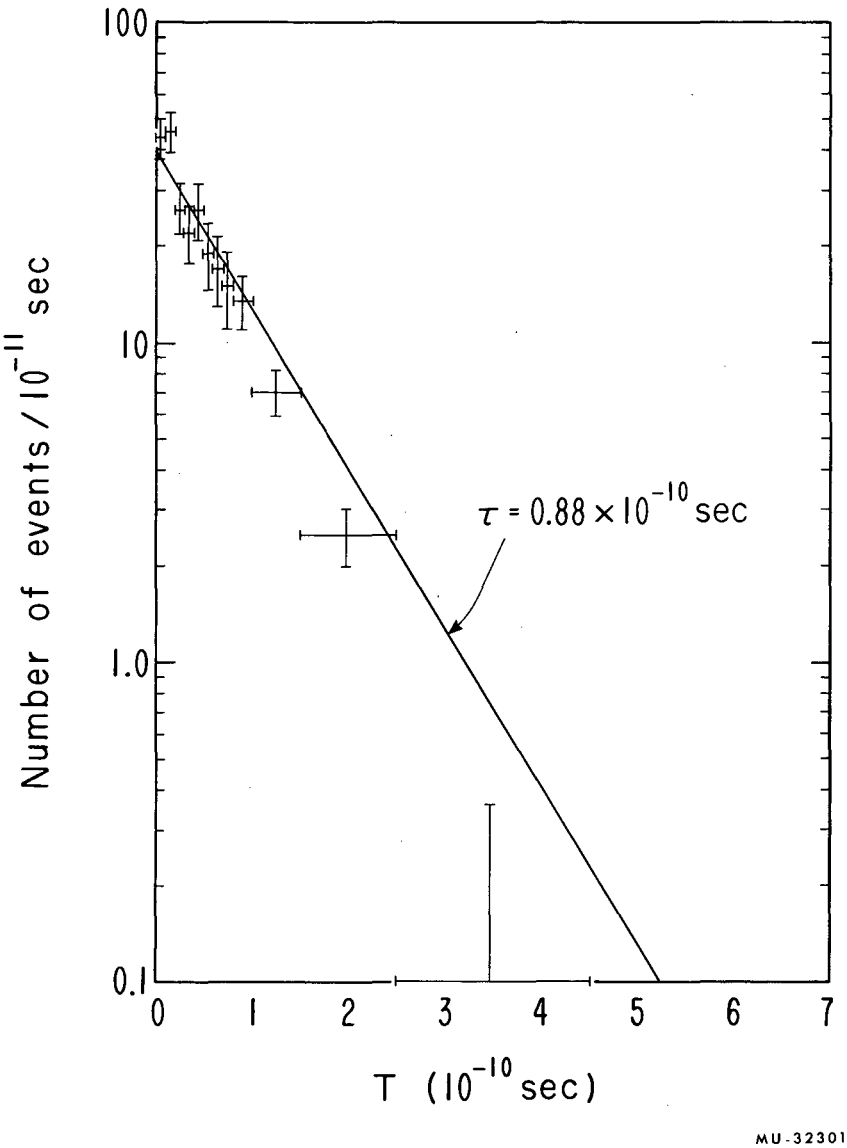

Fig. 5. Lifetime distribution of the K_1^0 decays for the corrected number of events.

In these selected rolls, the events were measured and processed by the kinematical fitting programs. The results of the computer analysis were then used by a physicist at the scanning table to select the proper final state.

To determine the cross section for events in class (c), we have normalized the number of events in that class that fit the final state $K^+ + p \rightarrow K^0 + \pi^+ + p$ to the cross section determined from the events in class (b). In order to use this event type we must subtract the number of K_1^0 that decay in the two-charged-pion decay mode outside the chamber and also must divide the number of events by the probability that an event will produce a K^0 that will not decay via the K_1^0 two-charged-pion decay mode in the chamber. The correction for the number of K_1^0 is based on the average correction found for the class (b) events. It was necessary to subtract 10 events from the number found in class (c).

The inelastic cross sections are given in Table I.

Table I. Cross sections observed for the K^+p interaction at 1.96 BeV/c.

Reaction product	Cross section (mb)
K^+p elastic	7.6 ± 1.0
$K^0\pi^+p$	4.6 ± 0.6
$K^+\pi^0p$	2.0 ± 0.3
$K^+\pi^+n$	1.6 ± 0.3
$K^+\pi^-p\pi^+$	1.7 ± 0.2
$K^0\pi^0p\pi^+$	1.3 ± 0.2
$K^0\pi^+n\pi^+$	0.33 ± 0.1
$K^+\pi^0p\pi^+$	~ 0.2
$K^+\pi^0n\pi^+$	~ 0.1
$K^+\pi^-\pi^0\pi^+p$	0.05 ± 0.02
$K^0\pi^+\pi^-\pi^+p$	0.02 ± 0.01
$K^+\pi^-\pi^+\pi^+n$	0.01 ± 0.006
$K^+K^+\Lambda$	$\lesssim 0.01$
$\sigma_{total.}$	19.5 ± 2.1

B. Double Pion Production

In order to study the two-pion production in the reaction $K^+ + p \rightarrow K^+ + \pi^- + \pi^+ + p$, we find it convenient to present the data in a phase-space triangle. The details of such a triangle are discussed in Appendix A. The three possible pairings of the particles in the final state are shown in Figs. 6, 7, and 8. In Fig. 6 we see direct evidence for the domination of the reaction by the K^* and N^* resonances. We also note that if we define events with the invariant mass of the π^- and the K^+ between 840 and 940 MeV as being within the K^* resonance, and events with the invariant mass of the π^+ and the proton between 1130 and 1300 MeV as being within the N^* resonance, 64% of the events lie within the double resonance. Figure 7 corresponds to observing a deviation of approximately 10% from phase space in the N^{*0} channel. We see no evidence for existence of any resonance in the isospin 3/2 of the K-π system, and thus confirm the earlier results, which had indicated a value of 1/2 for the isospin of the K^* resonance.[14] Figure 8 shows no evidence for production of the ρ^0 meson, which is restricted by phase space. There is no evidence for any resonance in the K^+p I = 1 state. It is noteworthy that production of the resonances in the K^*N^* system does not produce any deviation from phase space in the other channels, which reflects the nonexistence of any strong resonances between the other particle pairs within the kinematic limits of this experiment.

The domination of this final state by the K^* (I = 1/2) and N^*(I = 3/2) is also confirmed by examining the other charge modes for double pion production. The final states are listed in Table II, along with the observed number of events and the number predicted by assuming that the final state is a pure mixture of isotopic spin 3/2 for the π-N system and 1/2 for the π-K system. The results indicate that the final state is completely dominated by the production of the two resonances.

In an earlier result of this experiment,[5] we determined the spin of the K^* to be 1 by performing an Adair analysis on those events

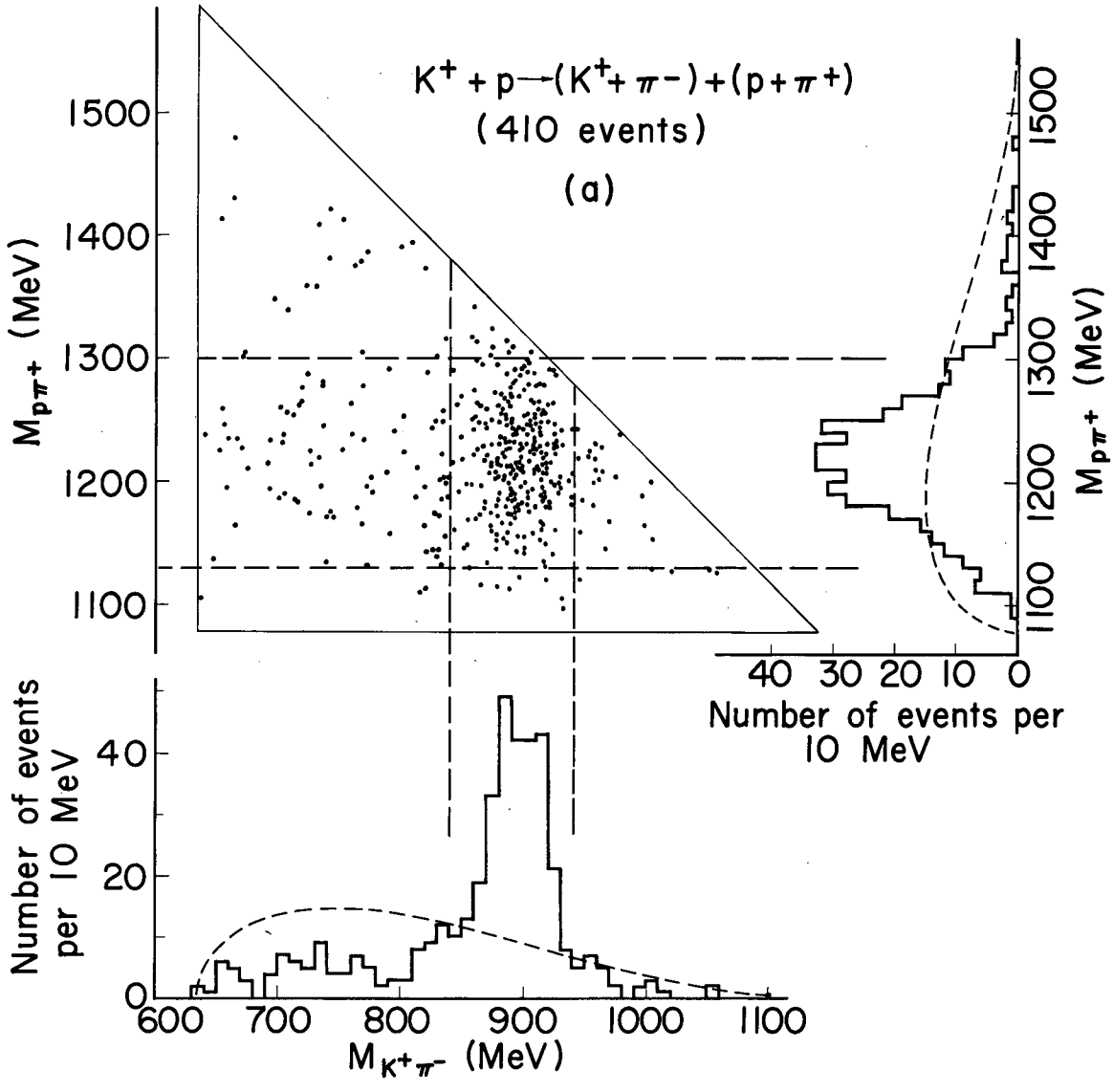

Fig. 6. Invariant mass distribution for the $K^+\pi^-$ and $p\pi^+$ pairs.

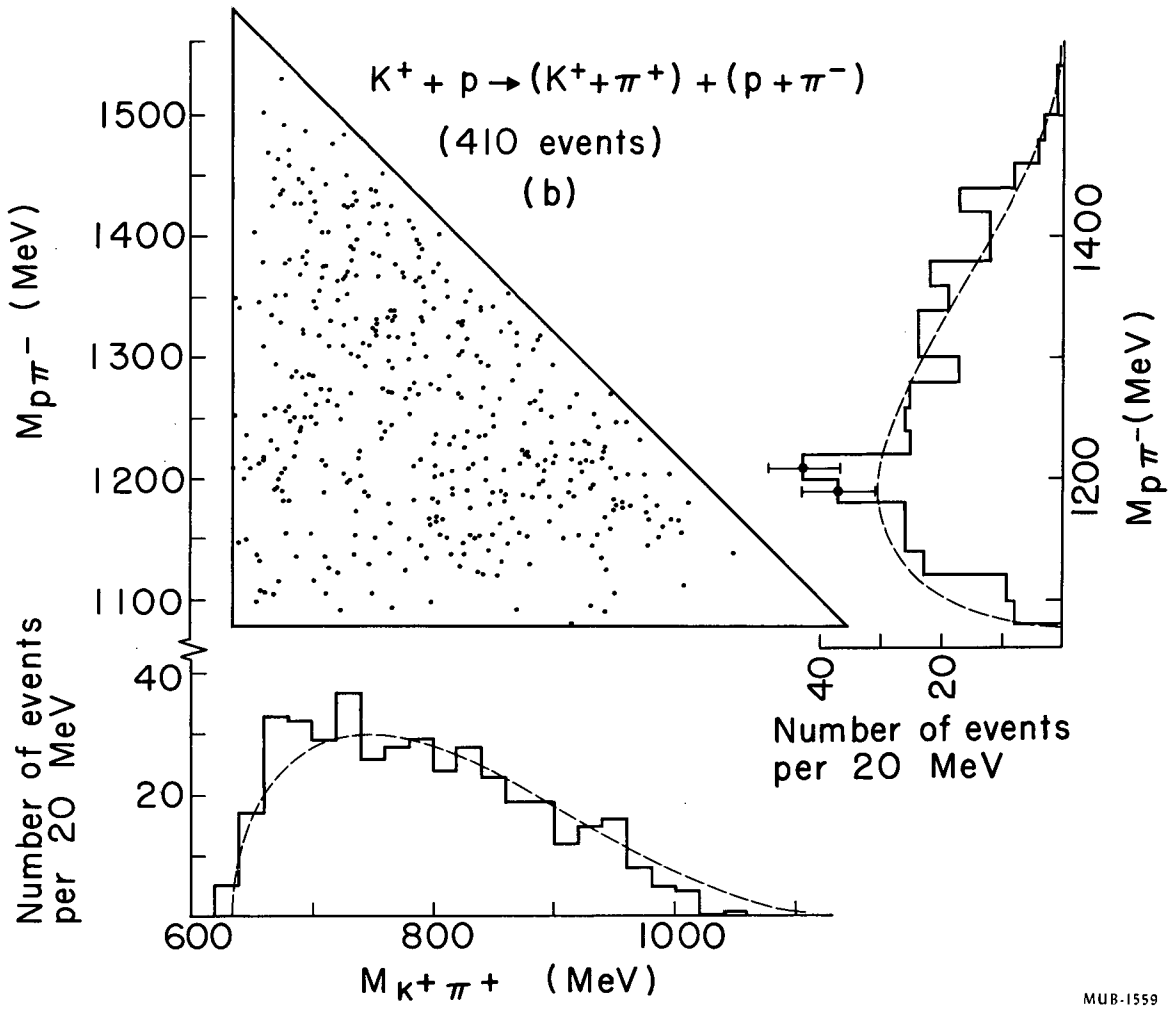

Fig. 7. Invariant mass distribution for the $K^+\pi^+$ and $p\pi^-$ pairs.

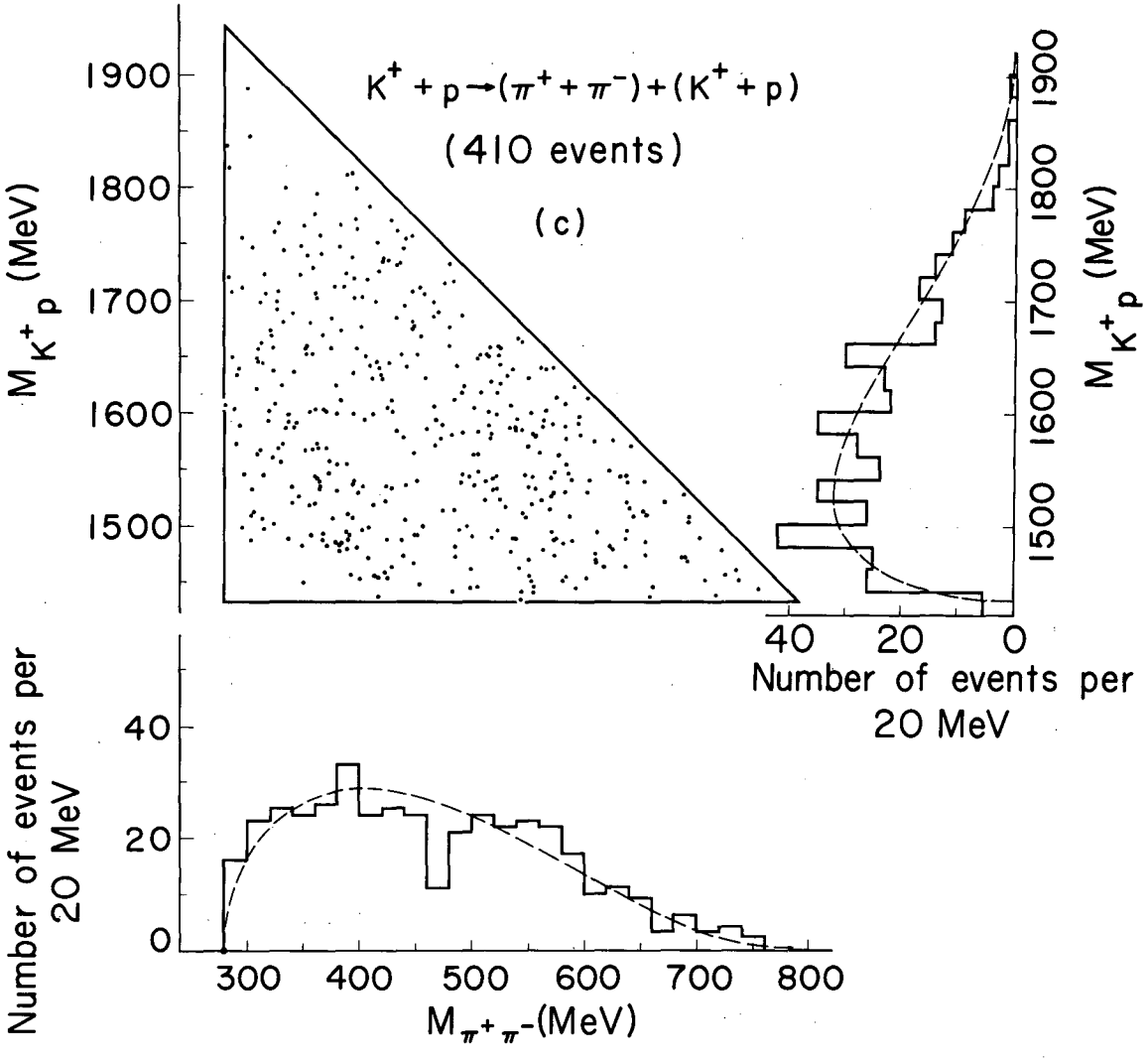

Fig. 8. Invariant mass distribution for the $\pi^+\pi^-$ and K^+p pairs.

Table II. Distribution of events in the four-particle final state.

Final state	Events observed	Events corrected	Percent in final state	Percent predicted by pure K^*N^* final state
$K^+\pi^-p\pi^+$	425	425	52.4	52.9
$K^0\pi^0p\pi^+$	103	309	38.1	38.2
$K^0\pi^+n\pi^+$	26	78	9.5	8.9

within the double-resonance region for which the cosine of the production angle of the K^* is greater than 0.8. Spin 1 was assigned because the observed angular distribution of the K^+ from the K^* decay was consistent with a pure cosine-squared distribution. Since Alston et al.[14] had previously offered evidence that the K^* spin must be less than 2, it is clear that the spin must be 1 and that we are observing an alignment in the $m_z = 0$ state. The observed alignment of the K^+ from the K^* decay can be understood by noting that, at the energy of this experiment, the Adair angle does not differ greatly from the $K^+_{in} - K^+_{out}$ angle in the rest frame of the K^*. The observed alignment results from the scattering of the kaon by another spinless particle. Since both particles are spinless, we cannot define any other axis except the incoming direction, and the scattering is completely specified by $P_1(\cos\theta)$. The most reasonable explanation, then, would be that the reaction is dominated by the one-pion exchange.

A test of the one-pion exchange was proposed by Treiman and Yang[15] and is illustrated in Fig. 9. The test is made in a reference frame in which one of the particles in the initial state is at rest. The angle ϕ is defined by

$$\phi = \cos^{-1} \left(\hat{K}_1 \times \hat{q} \cdot \hat{K}_5 \times \hat{K}_6\right),$$

$$\bar{q} = \bar{K}_1 - \bar{K}_4 - \bar{K}_3,$$

and

$$\bar{K}_2 = 0,$$

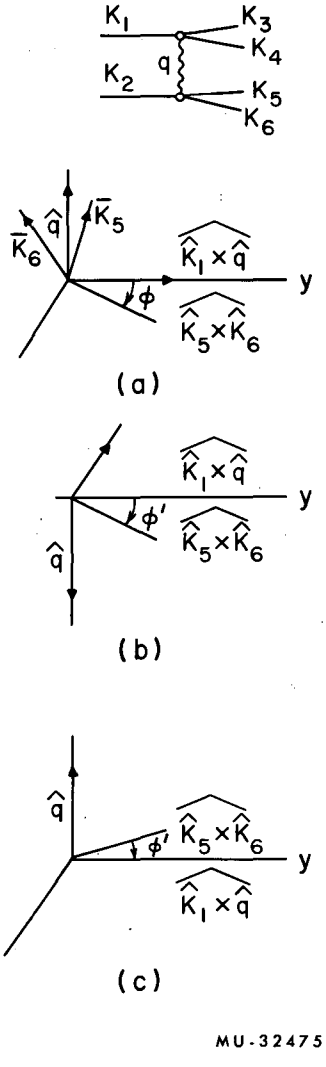

Fig. 9. Treiman-Yang test. (a) Defined for the diagram at the top of the figure. (b) After parity inversion. (c) After rotation about the y axis.

and is illustrated in Fig. 9a. Since the intermediate particle is spinless, the distribution in ϕ must be isotropic. Figure 9b shows the same case after parity inversion. To compare it with case (a), we must rotate the system 180 deg about the y axis, as shown in (c). It is clear that since strong interactions are invariant under parity inversion, we need examine only the angular distribution from 0 to 180 deg.

In Fig. 10 we show the Treiman-Yang test for our data as performed in the laboratory system and in the rest frame of the incoming K^+. The shaded part corresponds to the double-resonant region we have previously defined. As can be seen, all distributions are consistent with being isotropic. It should be borne in mind that the Treiman-Yang test is a necessary, but not sufficient, test of the one-pion-exchange model.

To test the one-pion-exchange model, we have studied the virtual scattering angle of the K^+ in the K^* rest frame, α, as a function of the momentum transfer for the events in the double-resonant region. The distribution is shown in Fig. 11. The striking feature is that the distribution can be fitted by a pure cosine-squared term for momentum transfers as great as 25 m_π^2. Beyond this limit the distribution approaches isotropy. In Fig. 12 we also examine the virtual scattering angle of the pion at the N^* vertex. Here the distribution is expected to be $1 + 3\cos^2\beta$, where β is the scattering angle. The data in this case are not conclusive. Although they are consistent with the predicted distribution shown on the graph, they are also consistent with being isotropic.

Therefore, using the K^* as an analyzer and examining the virtual scattering angle of the K^+ in the K^* rest frame, we conclude that the reaction $K^+ + p \rightarrow K^* + N^*$ is completely consistent with the one-pion-exchange model for momentum transfers as high as 25 m_π^2.

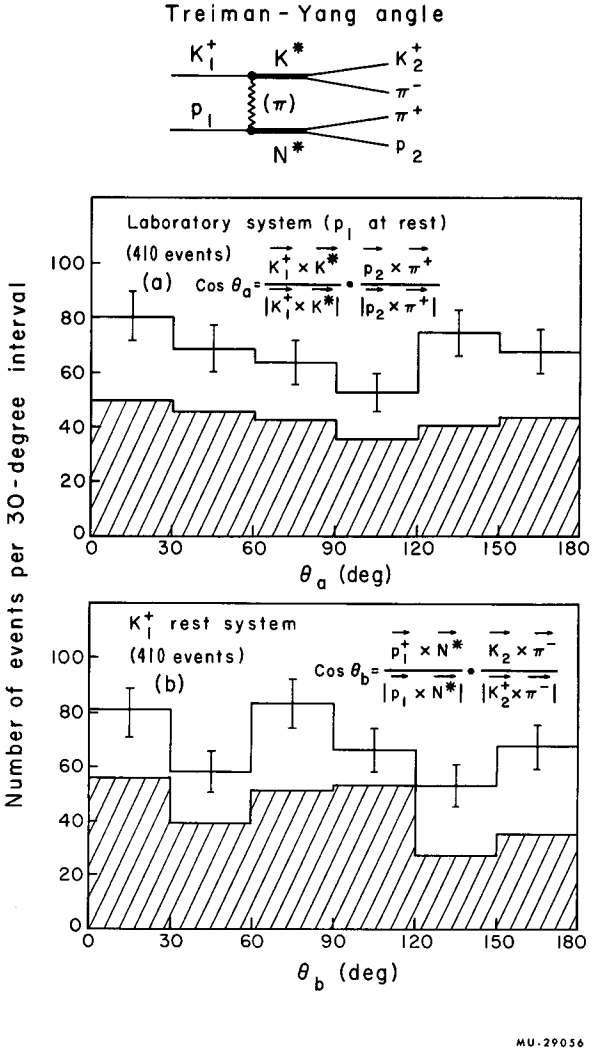

Fig. 10. Treiman-Yang test for the experimental data. (a) In the laboratory system. (b) In the rest system of the incoming K^+.

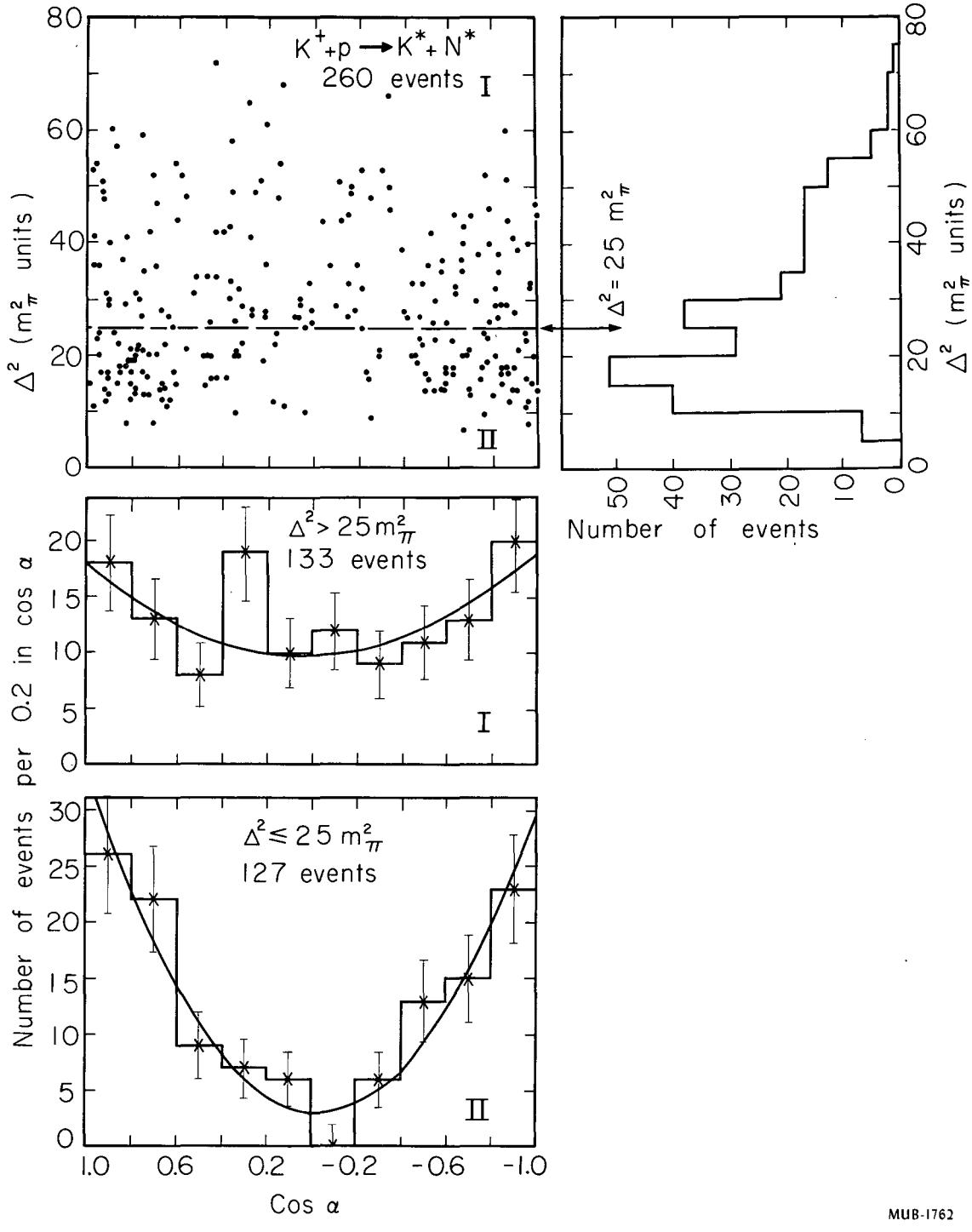

Fig. 11. Virtual scattering angle, α, as a function of the momentum transfer.

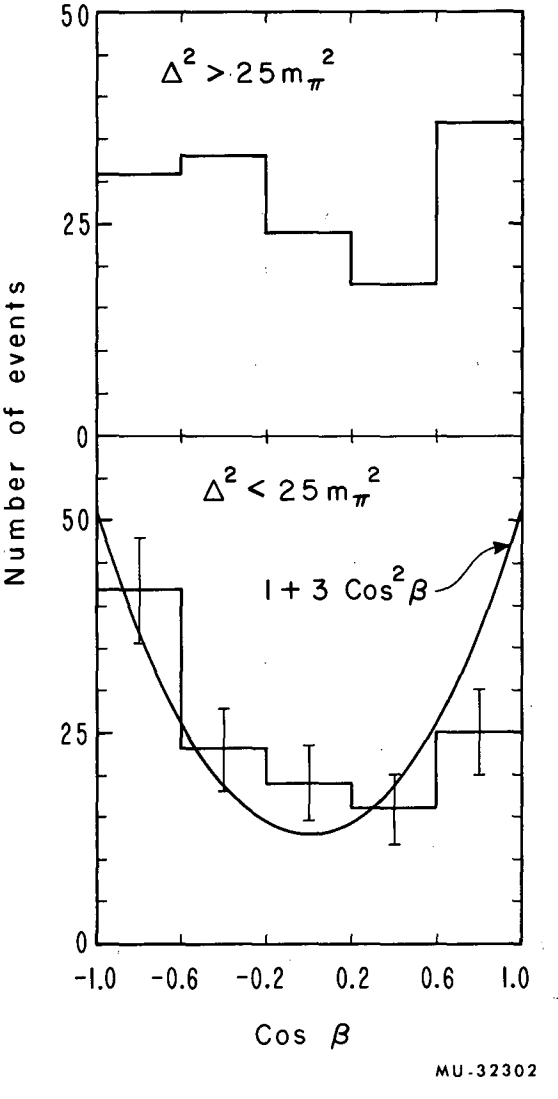

Fig. 12. Virtual scattering angle, β, as a function of the momentum transfer.

C. Single-Pion Production

At 1.96 BeV/c, single-pion production by K^+ mesons can proceed by three channels:

(a) $K^+ + p \rightarrow K^0 + \pi^+ + p$,

(b) $K^+ + p \rightarrow K^+ + \pi^0 + p$,

(c) $K^+ + p \rightarrow K^+ + \pi^+ + n$.

In Fig. 13 we show the Dalitz plots for the three reactions. For reaction (a) we have shown only events not accompanied by K_1^0 decay into two charged pions. Reactions (a) and (b) can proceed via K^* + N production or via K + N^* production. Reaction (c) can proceed only via K + N^* production. The domination of the resonances in the pion production is shown clearly in the Dalitz plots.

To examine this in more detail we limit the discussion to reaction (a), for which we have the largest number of events. In Fig. 14 we combine the events from the previous figure with the events that gave a charged-pion mode of decay for the K_1^0.

In Fig. 15 we show the distribution of the production angle for π-N mass combinations in the N^* resonance limits and for π-K mass combinations in the K^* resonance limits. We have not at this point attempted any separation of the events in the interference region of the resonances; hence, some events appear in both distributions. Peaking of the resonances in the forward direction for the K^* (or backward for the N^*) indicates that the resonances are produced peripherally and may proceed via a one-particle-exchange mechanism as indicated on the diagrams above the figure. If the reaction does proceed via the single-particle exchange, then the N^* production may differ from the K^* production, since the one-pion exchange is forbidden owing to parity considerations at the K^+ - K^0 vertex, whereas it is allowed for K^* production.

To examine this further we have attempted to separate the K^* events from the N^* events in the interference region. Examining the Dalitz plot for this reaction, Fig. 14, we see no constructive interference between the two processes. The number of events in the interference region appears to be a linear superposition of the events

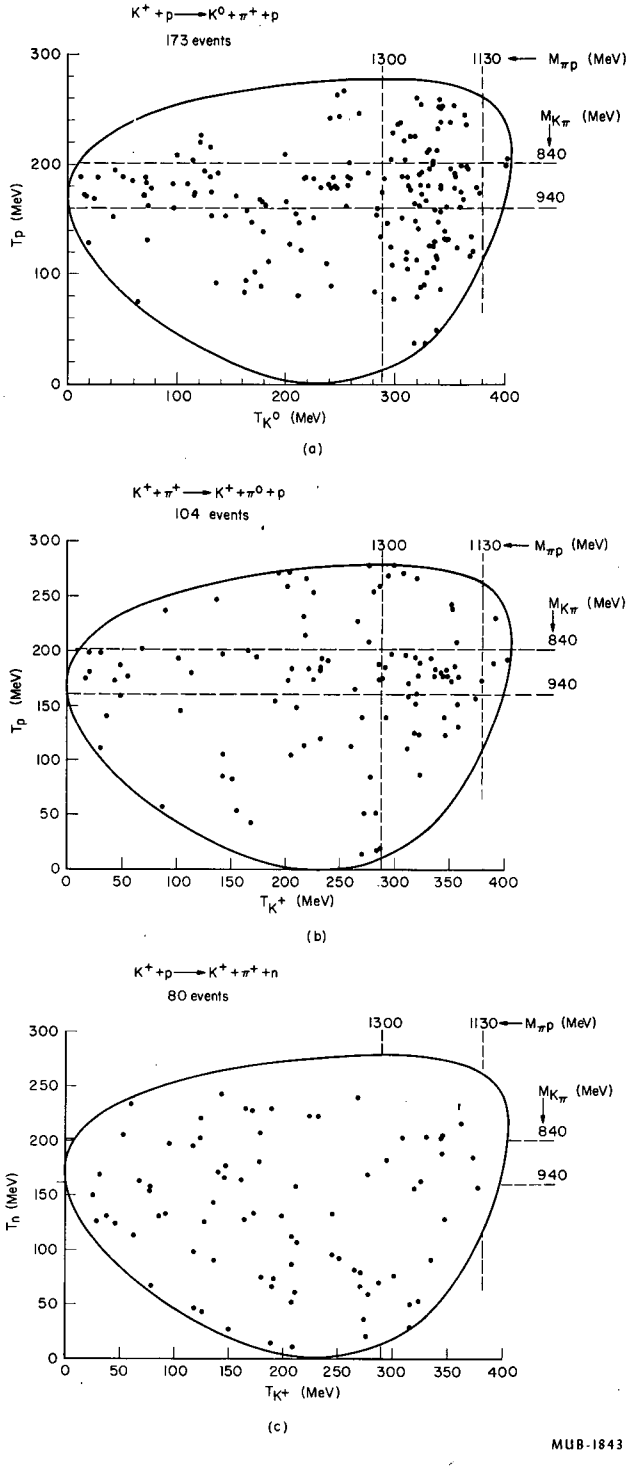

Fig. 13. Dalitz plots for the three body final states.

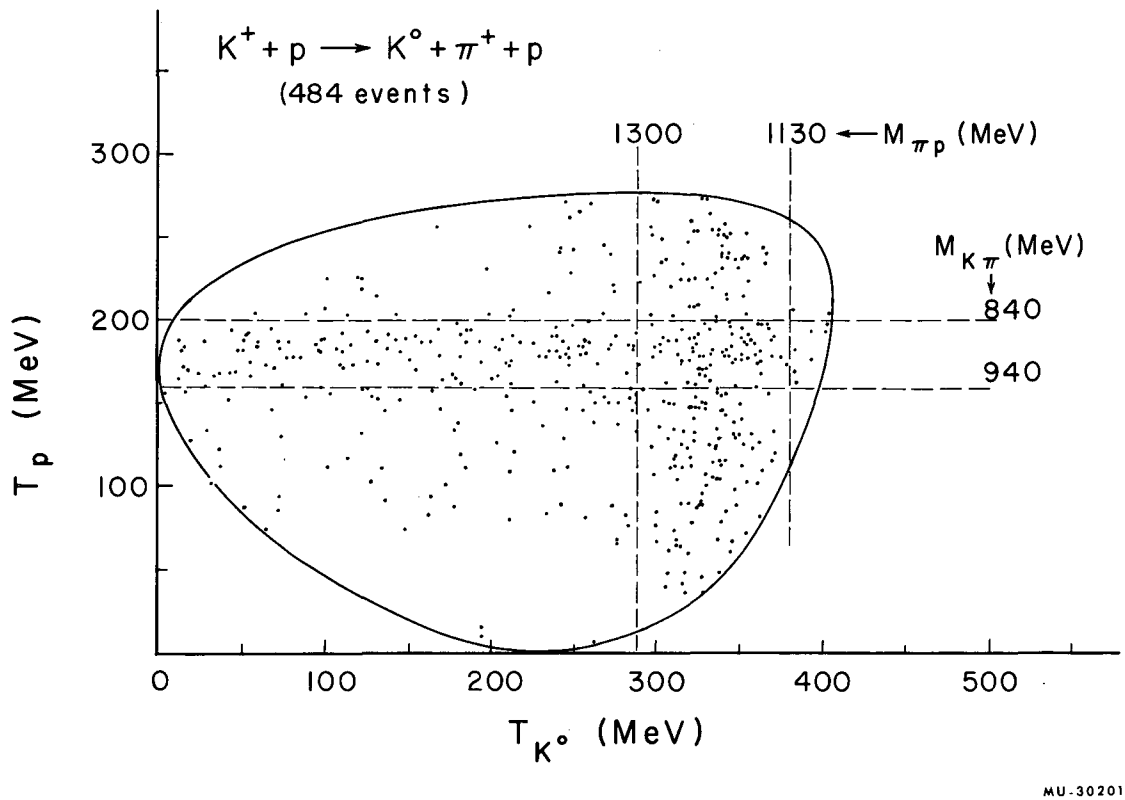

Fig. 14. Dalitz plot for the reaction $K^+ + p \rightarrow K^0 + \pi^+ + p$.

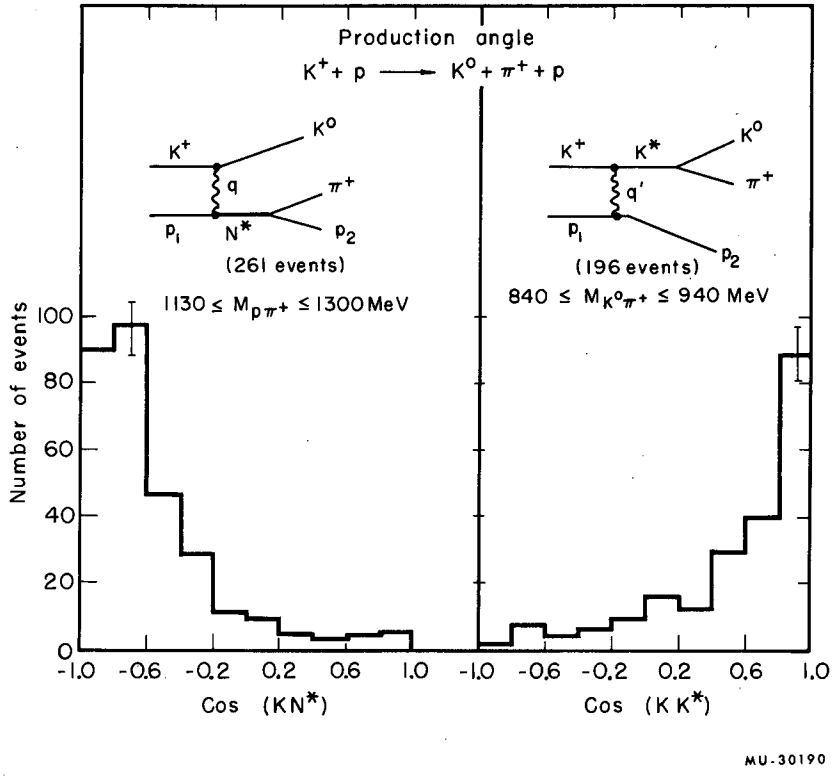

Fig. 15. Production-angle distributions for the N^* and the K^*.

in each resonance band. The distribution of the production angle of the pion is given in Fig. 16 for the three regions, the interference region and each of the resonance regions minus the interference region. It is seen that the production-angle distribution of a pion produced with a K^* is peaked in the forward direction, while the production-angle distribution of a pion associated with an N^* is peaked in the backward direction. Therefore, we have assigned the particles in the interference region to the K^* or the N^* region, based on whether the pion goes backward or forward, and on the proximity to the nominal resonance central value. In the subsequent histograms, the shaded area shows the result of subtracting such events.

In Figs. 17 and 18 we show the Treiman-Yang test for K^* and N^* production, with the peripheral diagram above the distribution. The significant point is that although the K^* distribution exhibits at most a slight deviation from an isotropic distribution, the N^* distribution shows a strong deviation. The distribution may be fitted by

$$f(\phi) = a + b\cos(\phi) + c\cos^2(\phi).$$

Performing a least-squares fit to the data, we find

$$a = 5.0 \pm 0.4,\ b = -0.4 \pm 0.25,\ \text{and}\ c = -3.0 \pm 0.6.$$

The observed alignment indicates the exchange of a vector meson. Since the exchanged meson must be charged, the nearest pole would be the ρ meson. Stodolsky and Sakurai have calculated the Treiman-Yang distribution based on an analogy between N^* production by a virtual photon which is dominated by a pure magnetic-dipole transition ($M1 \rightarrow P_{3/2}$) and N^* production by a virtual vector meson.[16] They conjecture that the vector-meson-exchange model will also be dominated by a pure $M1 \rightarrow P_{3/2}$ transition, and predict values for the Treiman-Yang angular distribution of $b/a = 0$ and $c/a = -0.67$. The observed values are $b/a = -0.08 \pm 0.05$ and $c/a = -0.6 \pm 0.13$. Similar results have also been reported independently by Kehoe for this reaction at 910 MeV/c.[17]

Further analysis of these events is in progress, and the final results will be presented at a future time.

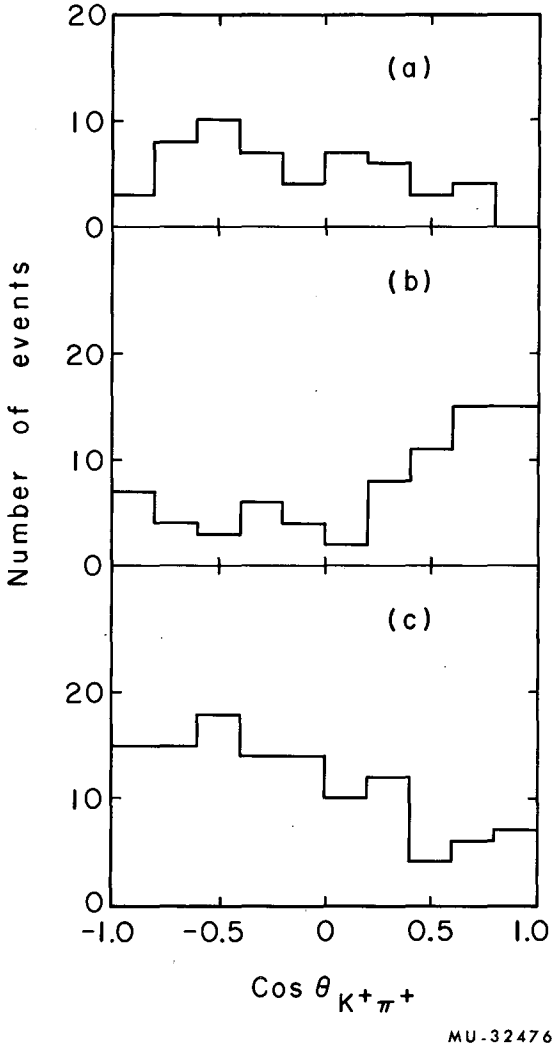

Fig. 16. Production angle of the π^+. Distribution (a) is for the interference region, distribution (b) is for the K^* band minus the interference region, and distribution (c) is for the N^* band minus the interference region.

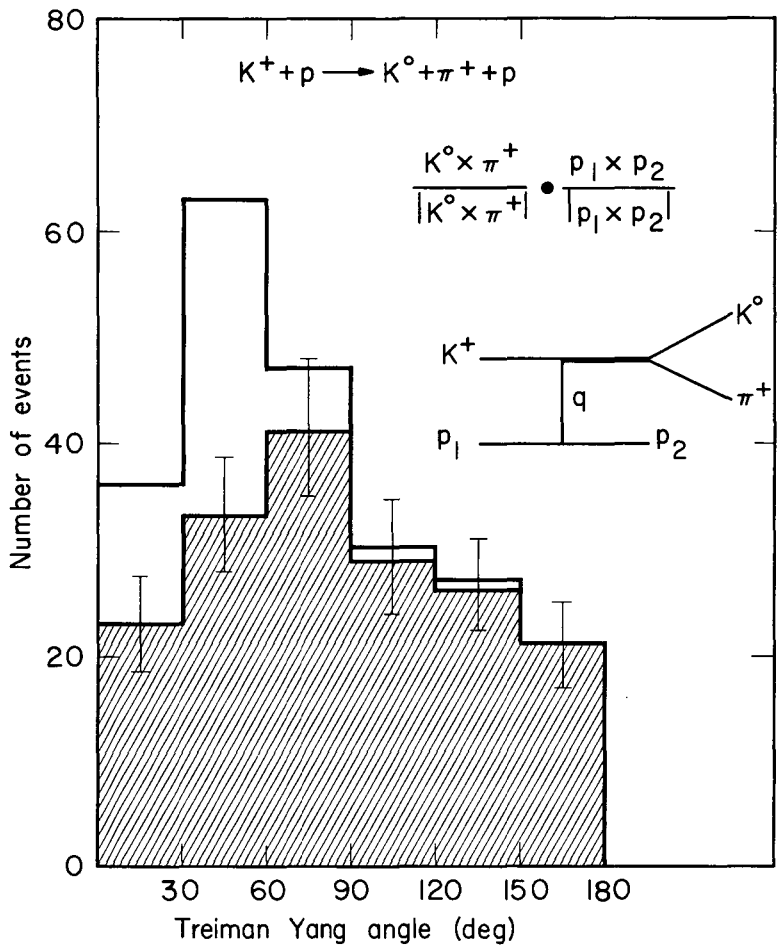

Fig. 17. Treiman-Yang distribution for $K^+ + p \rightarrow K^* + p$.

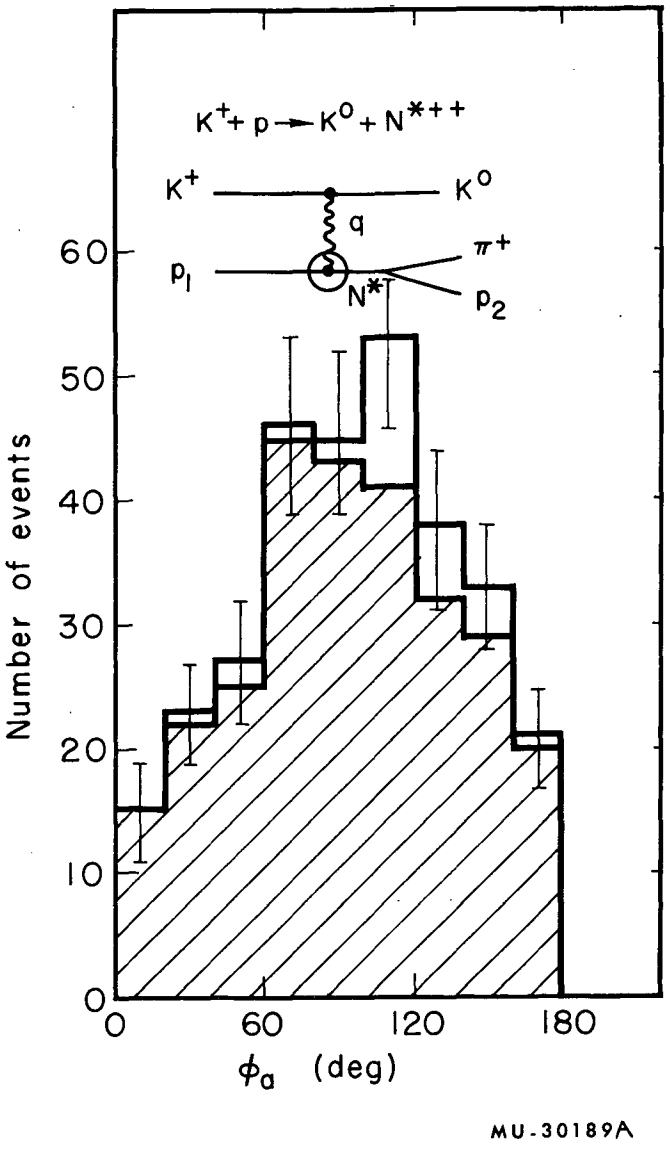

Fig. 18. Treiman-Yang distribution for $K^+ + p \rightarrow K^0 + N^*$.

IV. THE ONE-PION-EXCHANGE MODEL

The first proposal to utilize single-particle-exchange diagrams was made by Chew and Low.[18] They proposed measurement of cross sections normally unavailable to the experimenter (e.g., π-π, e-π, etc.) by employing the physical principle of the existence of poles in the S matrix corresponding to the exchange of single-particle intermediate states.

Several authors subsequently proposed that the single-particle-exchange pole would probably also dominate the reaction when the pole is close to the physical region.[4] The Salzmans emphasized that the virtual pion behaved as an incoming particle at each vertex in the rest frame of that vertex and formulated the one-pion-exchange model in terms of virtual or off-the-mass-shell cross sections. The virtual cross section was defined as the ratio of the transition probability for the virtual interaction to the invariant flux.

Recently Ferrari and Selleri have studied single-pion production by nucleon-nucleon interactions and have succeeded in fitting the experimental data at several energies by introducing a form factor into their single-pion-exchange calculations.[19] Berman has also calculated the one-pion exchange for the reaction $K^+ + p \rightarrow K^* + N^*$ by considering the K^* and the N^* as particles and expressing the differential cross section as simply the inelastic production of the two particles via one-pion exchange.[20] In Appendix B we show that this is equivalent to the Salzmans' formulation in the limit as the width of the resonances becomes small.

In the preceding section of this dissertation the results of the analysis of the reaction $K^+ + p \rightarrow K^* + N^*$ indicated that the one-pion exchange dominated the reaction for momentum transfers as high as $25\ m_\pi^2$. In this section we discuss the one-pion exchange, using the formulation of the Salzmans. In the calculation it is clear that by taking into account the spin of the K^* and the N^* and the virtuality of the interaction, we must introduce a function dependent on the momentum transfer to fit the data.

In Appendix B we show that the total cross section is given by

$$\sigma_{K^+ + p \to K^+ + \pi^- + p + \pi^+} = \frac{2}{(2\pi)^3 P_{iu}^2 U^2} \int \frac{K_{K\pi} M_{K\pi}^2 \sigma(M_{K\pi}, \Delta^2) K_{\pi p} M_{\pi p}^2}{(\Delta^2 + m_\pi^2)^2}$$

$$\times \sigma(M_{\pi p}, \Delta^2)\, dM_{\pi p}\, dM_{K\pi}\, d\Delta^2,$$

where K_{ij} is the three-momentum in the ij rest frame, M_{ij} is the invariant mass of ij, Δ^2 is the square of the four-momentum transfer, P_{iu} is the momentum of the K^+ in the center of mass of the initial state, U is the total center-of-mass energy, and $\sigma(M_{ij}, \Delta^2)$ is the cross section of the virtual reaction for a total energy of M_{ij} and a momentum transfer of Δ^2. The result of the above equation must be multiplied by a factor of 2/3 in order to allow for the neutral decay mode of the K^*.

In Appendix B we show that as a first approximation the fact that the pion is off the mass shell for a p-wave resonance changes the momentum dependence of the matrix element. Therefore, following the Salzmans[6] and Selleri,[21] we have conjectured that the virtual scattering cross section is given by

$$\sigma(M_{ij}, \Delta^2) = \left[\frac{p^{off}}{p^{on}}\right]^2 \sigma(M_{ij}),$$

where p^{off} is the off-the-mass-shell momentum in the ij rest frame, p^{on} is the on-the-mass-shell momentum in the ij rest frame, and $\sigma(M_{ij})$ is the physical cross section for an invariant mass M_{ij}.

We use the Breit-Wigner formula to compute the physical cross section. For the width of the resonance, we have used

$$\Gamma = \frac{2 p^3 a^3}{1 + p^2 a^2} \gamma,$$

where p is the momentum of the pion in the rest system of the K^* or N^*, a is the scattering length, and γ is the reduced width.

The parameters for the N^* are given by Gell-Mann and Watson.[22] For the K^* we have fitted the $K^+\pi^-$ mass distributions. The best-fit parameters are

$$M_{K^*} = 896 \pm 4 \text{ MeV},$$

$$a = 0.8 \times 1/m_\pi,$$

and

$$\gamma = 18.5 \text{ MeV}.$$

In lieu of the errors on the scattering length, a, and the reduced width, γ, the boundaries of the shaded area on Fig. 19 correspond to the value of the minimum χ^2 plus one. The resonance width is consistent with a value of $\Gamma = 42 \pm 5$ MeV.

The cross section calculated by using these conjectures is approximately 30 mb, which is to be compared to the observed cross section of 1.1 mb. The experimental differential cross section, Fig. 20, is peaked in the forward direction, whereas the calculated cross section is almost isotropic.

In order to fit the data with these conjectures, a form factor must be introduced. We have chosen the factor

$$F(\Delta^2) = \frac{\Lambda^2 - m_\pi^2}{\Delta^2 + \Lambda^2},$$

where Λ is a parameter to be determined from the experimental data, and the integrand in the Salzman equation is multiplied by $F^2(\Delta^2)$. The choice of this factor is somewhat arbitrary. We have chosen a form similar to the nucleon form factor, which is normalized to one when the reaction is on the mass shell. The experimental differential cross section along with the calculated differential cross section is given in Fig. 20 for a value of $\Lambda = 3.4\, m_\pi$.

In Fig. 21 we show the mass plots along with the calculated curves corresponding to the one-pion exchange plus phase space. Agreement with the experimental data is good.

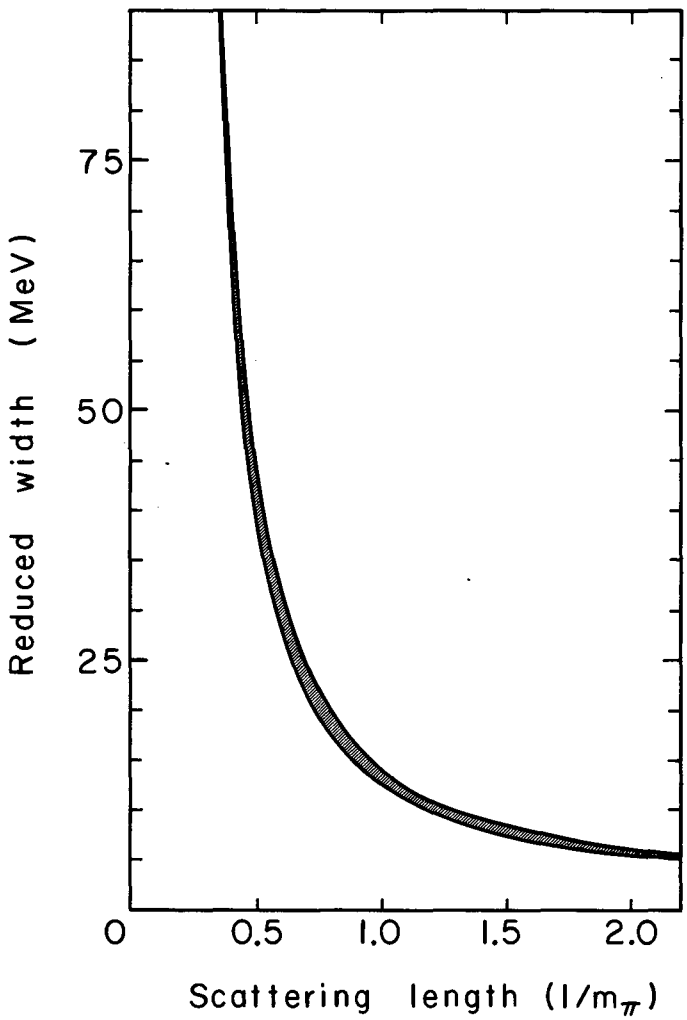

Fig. 19. Range of a, the scattering length, and γ, the reduced width, which fit the experimental data. The shaded area corresponds to the minimum χ^2 plus 1.

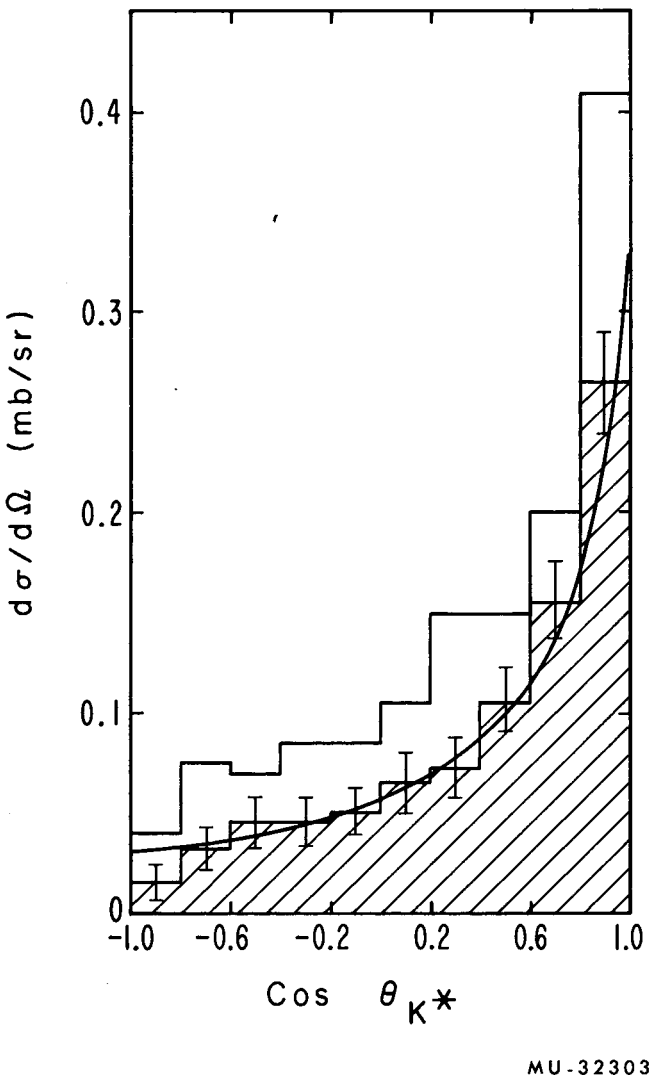

Fig. 20. Differential cross section for the reaction $K^+ + p \rightarrow K^* + N^*$. The curve is for $\Lambda = 3.4\ m_\pi$ in the form factor. The shaded area corresponds to events in the double resonance.

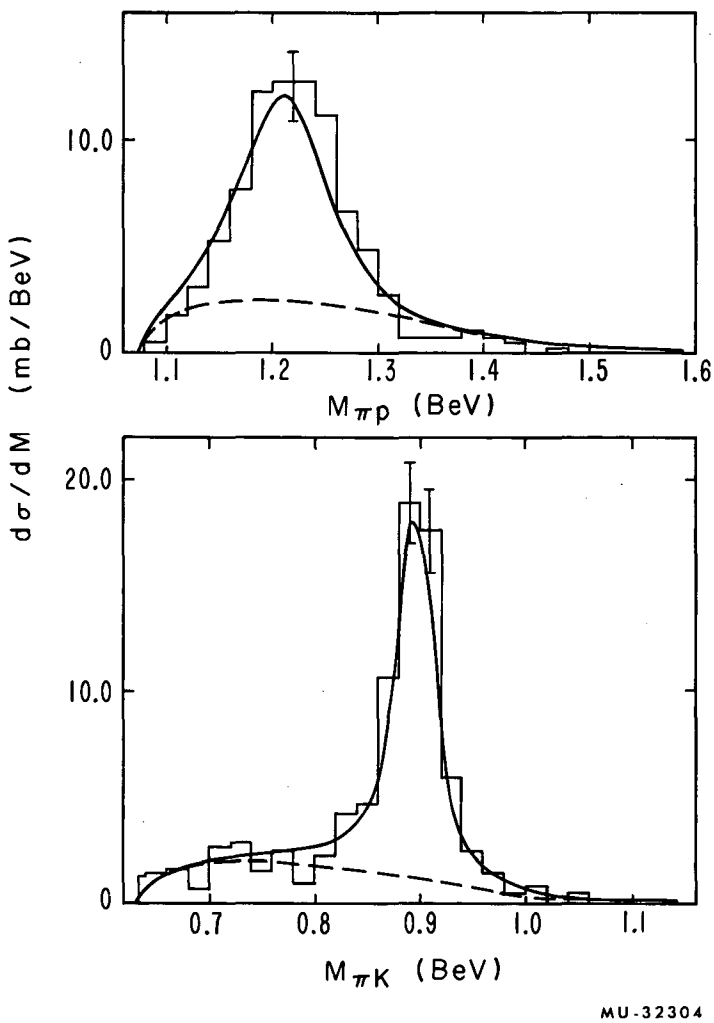

Fig. 21. Invariant Kπ and pπ mass distributions for the reaction $K^+ + p \rightarrow K^* + N^*$. The curve corresponds to a value of $\Lambda = 3.4\ m_\pi$. The dashed curve corresponds to a phase-space addition to the one-pion-exchange model.

It is interesting to examine the data from the original viewpoint of Chew and Low.[16] To do this we rewrite the Salzman equation as

$$\sigma(\Delta^2, M_{\pi p})\,\sigma(\Delta^2, M_{K\pi}) = \frac{(2\pi)^3 P_{iu} U^2 (\Delta^2 + m_\pi^2)^2}{2 K_{K\pi} M_{K\pi}^2 K_{\pi p} M_{\pi p}^2}$$

$$\times \left[\frac{d^3\sigma_{K^+ + p \to K^* + N^*}}{d\Delta^2\, dM_{\pi p}\, dM_{K\pi}}\right]_{\text{experimental}}$$

Such a plot is given for the intervals $865.0 \leq M_{K^*} \leq 915.0$ MeV and $1180.0 \leq M_{N^*} \leq 1270.0$ MeV in Fig. 22. For the small values of Δ^2 we see that the data are consistent with a linear extrapolation to the expected value for the product of the cross sections that is indicated on the graph.

The data can also be used to obtain the shape of the form factor itself. Since we can write

$$\sigma(\Delta^2, M_{\pi p})\,\sigma(\Delta^2, M_{K\pi}) = \left[\frac{p_{K\pi}^{\text{off}}\; p_{\pi p}^{\text{off}}}{p_{K\pi}^{\text{on}}\; p_{\pi p}^{\text{on}}}\right]^2 \sigma(M_{\pi p})\,\sigma(M_{K\pi})\,F^2(\Delta^2),$$

we can substitute into the original equation and obtain $F(\Delta^2)$. In Fig. 23 we show the data in this representation along with the form factor used. We note that, although we can say quite unambiguously that a form factor is needed, the data are not overly sensitive to the shape of the form factor. It would be interesting to repeat the experiment at higher energies, thus lowering the minimum kinematically allowed value of Δ^2. These are more sensitive to the shape of the form factor. We would also expect that if this form factor has any meaning, it would be independent of the energy of the incoming kaon; this could be tested by repeating the experiment at several energies.

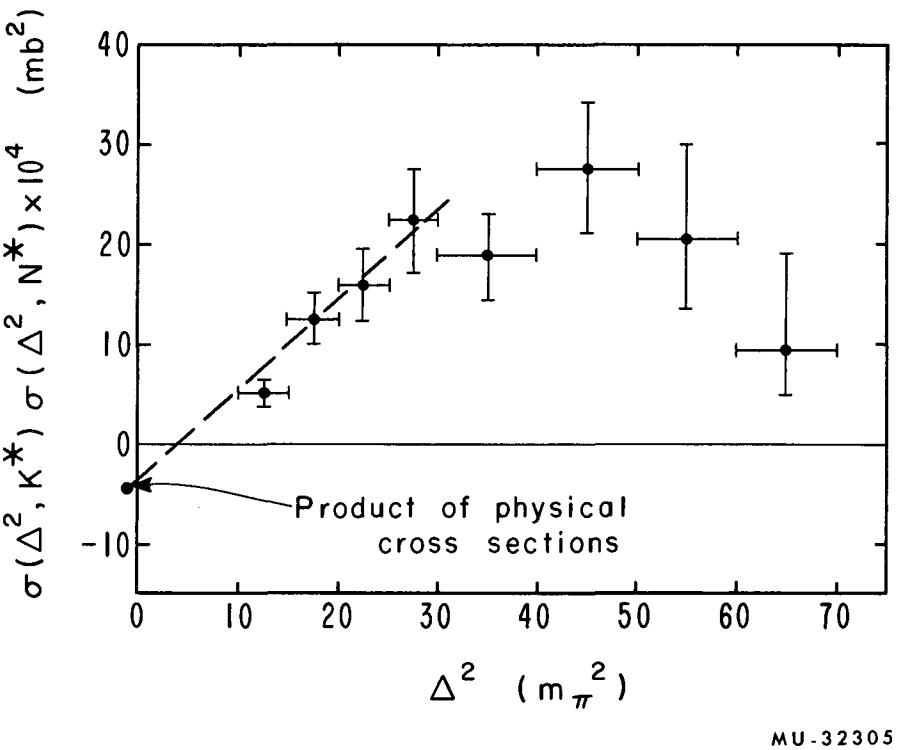

Fig. 22. Chew-Low plot for the reaction $K^+ + p \rightarrow K^* + N^*$. The data are for M_{K^*} = 865 to 915 MeV and M_{N^*} = 1180 to 1270 MeV.

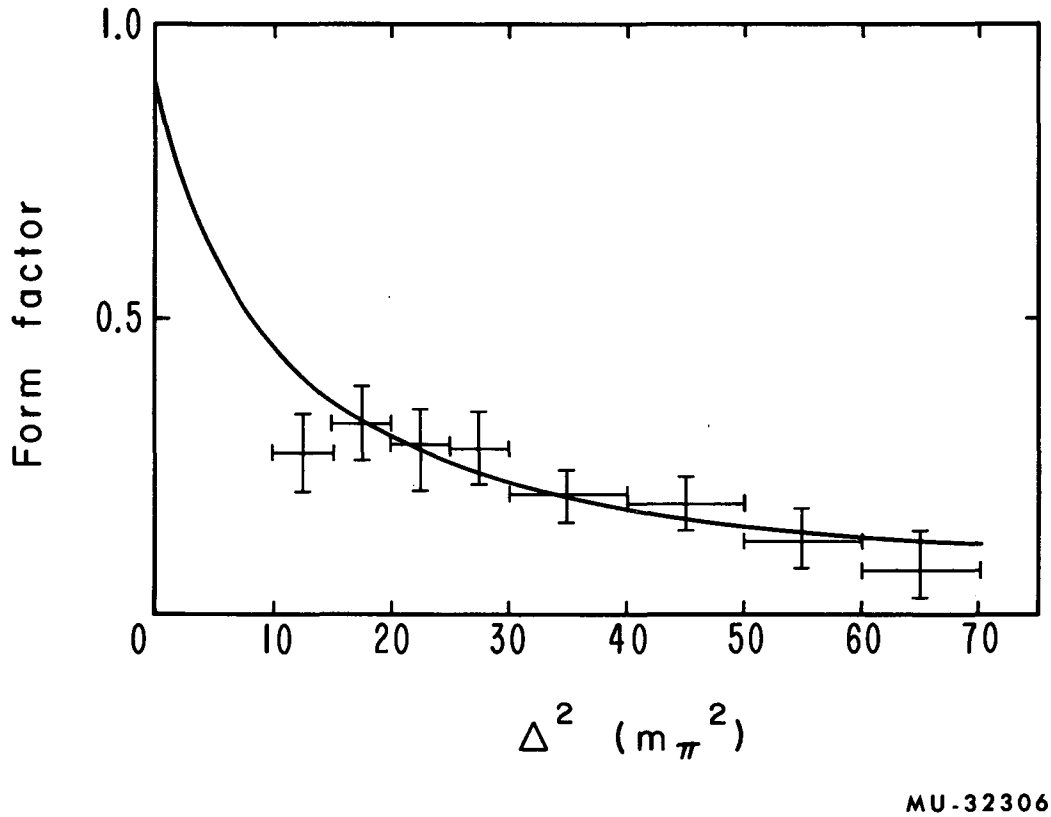

Fig. 23. Form factor versus the experimental data for M_{K^*} = 865 to 915 MeV and M_{N^*} = 1180 to 1270 MeV.

ACKNOWLEDGMENTS

I have been fortunate for the past few years to work under the guidance of Professor Gerson Goldhaber and Dr. Sulamith Goldhaber. I would like to express my sincere appreciation and gratitude to them for their encouragement and advice during the major part of my graduate studies.

I am indebted to Professor William Chinowsky for his advice and help both on this experiment and on other projects in the past few years.

I have benefited during the course of this work by many discussions with Professor Hans Peter Duerr and Professor Samuel M. Berman.

I would also like to express my gratitude to Dr. Ralph Shutt and the members of the Brookhaven National Laboratory's bubble chamber group along with the alternating-gradient synchrotron staff for their aid in making this experiment possible.

Many thanks are due Dr. Wonyong Lee and Dr. Theodore Stubbs, who were my coworkers on several projects over the past few years. In particular I would like to express my gratitude to Dr. Wonyong Lee for his aid during the course of this experiment.

I would also like to express my appreciation to Mr. Emmett Burns, Mr. Kirmach Natani, and Mr. James Miller for their aid in programming and operating the IBM 7090 computer during the course of this experiment.

The complicated bookkeeping and overall coordination required for the scanning and measurement of this film was accomplished by Mr. Joseph Gutierrez and Miss Harriet Rice. The secretarial tasks were performed by Mrs. Sally Wallace.

The scanning and measurement of this film were done by Mr. George Baker, Mrs. Lora Langner, Mr. Bryce Sheldon, Mrs. Frances Simon, Mr. George Swaney, Mrs. Lois Tinay, Mr. Jack Wells, and Mr. Russell Wills.

This work was done under the auspices of the U. S. Atomic Energy Commission.

APPENDICES

A. The Phase-Space Triangle

In considering the four-particle final state, it was found convenient to combine the particles into two invariant masses. That is, we consider

$$m_1 + m_2 \rightarrow \underbrace{m_3 + m_4}_{M_1} + \underbrace{m_5 + m_6}_{M_2},$$

where m_i is the rest mass of the particle and M_i is the invariant mass of the indicated pair.

In the M_1M_2 plane the kinematical limits for M_1 and M_2 form an isosceles right triangle, each side of length $U - m_3 - m_4 - m_5 - m_6$, where U is the total energy, and the hypotenuse is given by $M_1 + M_2 = U$. This is illustrated in Fig. 24.

The invariant phase space for the reaction is given by[23]

$$\Gamma_4(U) = \int \frac{d^3p_3\, d^3p_4\, d^3p_5\, d^3p_6}{2\omega_3\ \ 2\omega_4\ \ 2\omega_5\ \ 2\omega_6}\ \ \delta(p_1+p_2-p_3-p_4-p_5-p_6).$$

By rewriting the delta function as

$$\delta(p_1+p_2-p_3-p_4-p_5-p_6) = \int d^4P_1\, d^4P_2\, \delta(p_1+p_2-P_1-P_2)$$

$$\times\ \delta(P_1-p_3-p_4)\, \delta(P_2-p_5-p_6)$$

we may rewrite the phase space as

$$\Gamma_4(U) = \int \Gamma_2(M_1)\, \Gamma_2(M_2)\, d^4P_1\, d^4P_2\, \delta(p_1+p_2-P_1-P_2),$$

where the two-body phase space is given by

$$\Gamma_2(M_i) = \int \frac{d^3p_j\, d^3p_k}{2\omega_j\ \ 2\omega_k}\ \ \delta(P_i-p_j-p_k).$$

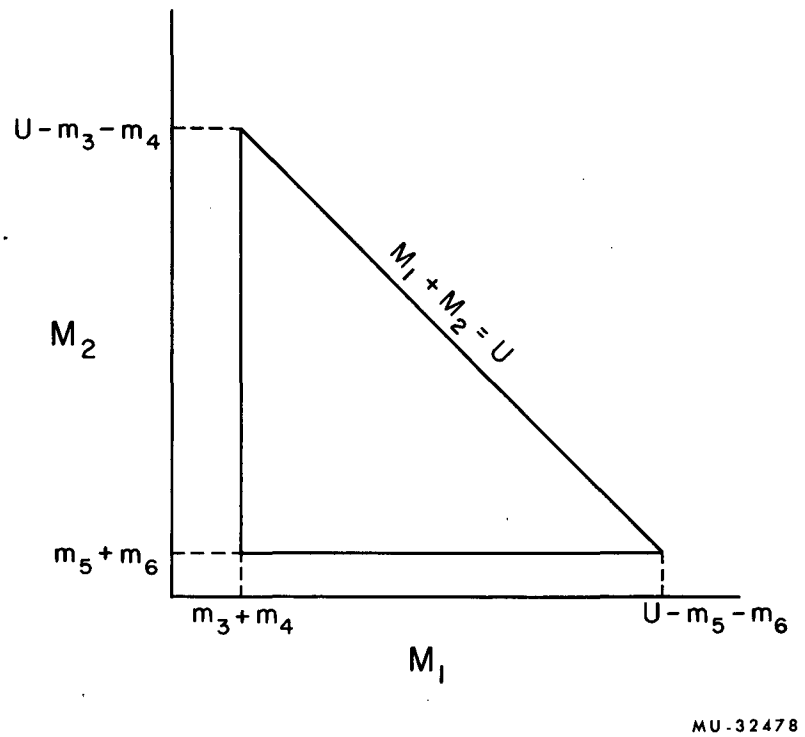

Fig. 24. Phase-space triangle.

Using the delta function to integrate over P_1, and using the equations

$$P_2^2 = \frac{(U^2 - M_1^2 - M_2^2)^2 - 4 M_1^2 M_2^2}{4 U^2}$$

and

$$W_2 = \frac{(U^2 - M_1^2 + M_2^2)}{2 U} ,$$

we find

$$d^4P_2 = 4\pi P_2^2 \, dP_2 \, dW_2 = \frac{\pi P_2}{U} \, dM_1^2 \, dM_2^2.$$

Therefore, we can express the phase space as

$$\Gamma_4(U) = \int \Gamma_2(M_1) \, \Gamma_2(M_2) \, \Gamma_2(U) \, dM_1^2 \, dM_2^2.$$

Here we have used the fact that two-body phase space is given by

$$\Gamma_2(M_i) = \frac{\pi p_i}{M_i} ,$$

where p_i is the rest-frame momentum of the decay products of M_i.

B. The One-Pion-Exchange Model

This appendix is in two parts. In the first part we formulate the one-pion-exchange model in the same manner as the Salzmans.[6] In the second part we show that in the limit as the widths of the resonances become small, the Salzmans' equation reduces to that formulated by Berman.

Using the notation in Fig. 25 we see that the matrix element for the interaction may be written as[24]

$$S = \frac{1}{(2\pi)^5} \left[\frac{m_p^2}{16 \omega_K \, \omega_p \, \omega_{K'} \, \omega_{\pi^+} \omega_{\pi^-} \omega_{p'}} \right]^{1/2} \frac{M_{K\pi} M_{p\pi}}{(\Delta^2 + m_\pi^2)}$$

$$\times \; \delta (P_K + P_p - P_{K'} - P_{p'} - P_{\pi^+} - P_{\pi^-}),$$

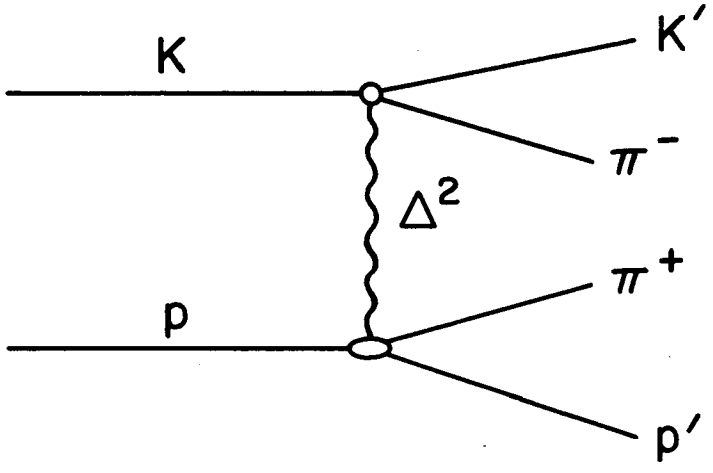

MU-32479

Fig. 25. One-pion-exchange diagram for the reaction $K^+ + p \rightarrow K^* + N^*$; $K^* \rightarrow K^+ + \pi^-$; $N^* \rightarrow \pi^+ + p$.

where $M_{K\pi}$ and $M_{p\pi}$ denote the matrix elements at the $K\pi$ and $p\pi$ vertices.

The cross section for the entire reaction is then given by

$$\sigma = \frac{m_p^2}{16(2\pi)^8 P_u U} \int \frac{|M_{K\pi}|^2_{av} \; |M_{p\pi}|^2_{av}}{\omega_{p'}\, \omega_{K'}\, \omega_{\pi^-}\omega_{\pi^+}(\Delta^2 + m_\pi^2)^2}$$

$$\times \; \delta(P_{K^+} + P_p - P_{K'} - P_{p'} - P_{\pi^+} - P_{\pi^-}) d^3p_{K'}\, d^3p_{p'}\, d^3p_{\pi^-} d^3p_{\pi^+},$$

where the subscript "av" stands for summing and averaging over the final and initial spin states.

An important observation by the Salzmans was that, since the virtual pion is spacelike, the pion behaves kinematically as an almost real pion at each vertex in the rest frame of the vertex (in this case the $K\pi$ or the $p\pi$). We can define, therefore, a virtual scattering cross section as the ratio of the virtual transition probability to the invariant flux. We have, therefore,

$$\sigma(M_{K\pi}, \Delta^2) = \frac{1}{16(2\pi)^2 P_{K\pi} M_{K\pi}} \int \frac{|M_{K\pi}|^2_{av}}{\omega_{K'}\; \omega_{\pi^-}} \; d^3P_{K'}\, d^3P_{\pi^-}\; \delta(P_{K\pi} - P_{K'} - P_{\pi^-})$$

and

$$\sigma(M_{p\pi}, \Delta^2) = \frac{m_p^2}{4(2\pi)^2 P_{p\pi} M_{p\pi}} \int \frac{|M_{p\pi}|^2_{av}}{\omega_{p'}\; \omega_{\pi^+}} \; d^3p_{p'}\; d^3p_{\pi^+}\; \delta(P_{p\pi} - P_{p'} - P_{\pi^+}).$$

Redefining the delta function in the same manner as in Appendix A, we may rewrite the cross section as

$$\sigma = \frac{4}{(2\pi)^4 P_{i\mu} U} \int \frac{\sigma(\Delta^2, M_{K\pi})\sigma(\Delta^2, M_{p\pi}) P_{K\pi} M_{K\pi} P_{p\pi} M_{p\pi}}{(\Delta^2 + m_\pi^2)^2}$$

$$\times \; d^4P_{K\pi}\, d^4P_{p\pi}\, (P_K + P_p - P_{K\pi} - P_{p\pi}).$$

Integrating by means of the delta function, we have

$$\sigma = \frac{2}{(2\pi)^3 P_{iu}^2 U^2} \int \frac{\sigma(\Delta^2, M_{K\pi})\sigma(\Delta^2, M_{p\pi}) P_{K\pi} M_{K\pi}^2 P_{p\pi} M_{p\pi}^2}{(\Delta^2 + m_\pi^2)^2}$$

$$\times \; dM_{K\pi}\, dM_{p\pi}\, d\Delta^2 \quad .$$

To relate the virtual cross section to the physical cross section we consider in detail the coupling of the incoming K meson and the virtual pion to the K^*. For simplicity we are concerned only with the coupling at the virtual-pion vertex. The matrix element in the rest frame of the K^* is proportional to $(\bar{P}_k - \bar{P}_\Delta)_j \bar{\epsilon}_j$, where we have written only the space components, as the polarization vector, $\bar{\epsilon}$, of the K^* is spacelike in the K^* rest frame. The transition probability has a term dependent on the momentum in the initial state, which in the case of a virtual interaction is given by

$$\left[p^{off}\right]^2 = \frac{(\Delta^2 + (M_{K^*} + M_{K^+})^2)(\Delta^2 + (M_{K^*} - M_{K^+})^2)}{4\, M_{K^*}^2} \quad ,$$

whereas physical scattering is evaluated with $\Delta^2 = -\, m_\pi^2$. We conjecture that the virtual cross section is related to the physical cross section by the relation

$$\sigma(\Delta^2, M_{K\pi}) = \sigma(M_{K\pi}) \left[\frac{p^{off}}{p^{on}}\right]^2 .$$

In computing the πp vertex we again work in the rest frame of the N^*. In this case we write the spin terms of the matrix element as a spinor and a four-vector coupled to the spin-3/2 wave function of the N^*. This can be written as

$$\bar{u}_2 (\bar{P}_p - \bar{P}_\Delta)_j \left[\frac{3\delta_{jk} - \sigma_j \sigma_k}{3}\right] \epsilon_k u_1,$$

where u_1 and u_2 are the N^* and proton spinors, respectively, $(\bar{P}_p - \bar{P}_\Delta)$ represents the relative momenta of the proton and pion in the final state, the term in brackets is the spin-3/2 projection operator, ϵ_k is the N^* polarization vector, and we have constructed the N^* wave function by coupling the spinor to the polarization vector and projected out the spin-3/2 part of the N^*. The transition probability is proportional to

$$(p^{off})^2 (\Delta^2 + (M_p + M_{N^*})^2).$$

We conjecture that the cross section is related to the physical cross section by

$$\sigma(M_{\pi p}, \Delta^2) = \sigma(M_{\pi p}) \left[\frac{p^{off}}{p^{on}}\right]^2 \frac{(\Delta^2 + (M_p + M_{N^*})^2)}{(-m_\pi^2 + (M_p + M_{N^*})^2)}$$

$$\approx \sigma(M_{\pi p}) \left[\frac{p^{off}}{p^{on}}\right]^2 .$$

As mentioned in the text, we have used Breit-Wigner formulas for the physical cross sections.

We now consider the entire reaction to go via the K^* and N^* resonances. Therefore, for the virtual cross sections we have

$$\sigma(M_{K\pi}, \Delta^2) = \frac{12\pi}{P_{K\pi}^2} \frac{\Gamma_{K^*}^2/4}{(M_{K^*}-M_{K\pi})^2+\Gamma_{K^*}^2/4} \frac{(\Delta^2+(M_{K^*}+M_K)^2)(\Delta^2+(M_{K^*}-M_K)^2)}{(-m_\pi^2+(M_{K^*}+M_K)^2)(-m_\pi^2+(M_{K^*}-M_K)^2)}$$

and

$$\sigma(M_{\pi p}, \Delta^2) = \frac{8\pi}{P_{\pi p}^2} \frac{\Gamma_{N^*}^2/4}{(M_{N^*}-M_{\pi p})^2+\Gamma_{N^*}^2/4} \frac{(\Delta^2+(M_{N^*}+M_p)^2)(\Delta^2+(M_{N^*}-M_p)^2)}{(-m_\pi^2+(M_{N^*}+M_p)^2)^2(-m_\pi^2+(M_{N^*}-M_p)^2)} .$$

We now consider a very narrow resonance. We rewrite the Breit-Wigner formula in the form

$$\frac{\Gamma_{N^*}^2 M_{N^*}^2}{(M_{N^*}^2 - M_{\pi p}^2)^2 + \Gamma_{N^*}^2 M_{N^*}^2} .$$

In the limit as Γ becomes small, the Breit-Wigner formula can be replaced by a delta function normalized to the same area:

$$\lim_{\Gamma \to \epsilon} \frac{1}{(M_{N^*}^2 - M_{\pi p}^2)^2 + \Gamma_{N^*}^2 M_{N^*}^2} = \frac{\pi}{\Gamma_{N^*} M_{N^*}} \delta(M_{N^*}^2 - M_{\pi p}^2) .$$

We also define the coupling constant for the N^* as[25]

$$\frac{g_{N^*}^2}{4\pi} = \frac{3}{2} \frac{\Gamma_{N^*} M_{N^*}^2}{p_{N^*}^3} .$$

The same substitutions may be made for the K^*.

Substituting these expressions into the Salzman equation and using the delta functions to perform the integrations over the mass spectrum, we have

$$\frac{d\sigma}{d\Omega} = \frac{\delta}{6} \frac{g_{K^*}^2}{S\,4\pi} \frac{g_{N^*}^2}{4\pi} \frac{1}{(\Delta^2 + m_\pi^2)^2}$$

$$\times \frac{[\Delta^2 + (M_{K^*}+M_K)^2][\Delta^2+(M_{K^*}+M_K)^2][\Delta^2+(M_{N^*}+M_p)^2]^2[\Delta^2+(M_{N^*}-M_p)^2]}{M_{K^*}^2 M_{K^*}^2[-m_\pi^2 + (M_{N^*}+M_p)^2]} ,$$

where

$$\delta = \frac{p_f}{p_i} = \left[\frac{[(S + M_{N^*}^2 - M_{K^*}^2)^2 - 4M_{N^*}^2 S]}{[(S + M_p^2 - M_k^2)^2 - 4M_p^2 S]}\right]^{1/2} ,$$

S is the square of the total energy, and we have used the substitution

$$d\Delta^2 = \frac{p_i\, p_f\, d\Omega}{\pi} .$$

This is a formula first derived by Berman, and represents the production of the K^* and N^* via one-pion exchange.

FOOTNOTES AND REFERENCES

1. F. Cerulus, Nuovo Cimento 14, 827 (1959).
2. W. Frazer and J. Fulco, Phys. Rev. 117, 1609 (1960).
3. M. Roos, Rev. Mod. Phys. 35, 314 (1963).
4. An extensive survey of the literature is given by E. Ferrari and F. Selleri, Nuovo Cimento 24, 453 (1962).
5. W. Chinowsky, G. Goldhaber, S. Goldhaber, W. Lee, and T. O' Halloran, Phys. Rev. Letters 9, 330 (1962).
6. F. Salzman and G. Salzman, Phys. Rev. 120, 599 (1960).
7. G. Goldhaber, W. Chinowsky, S. Goldhaber, W. Lee, and T. O' Halloran, Phys. Letters 6, 62 (1963); G. Goldhaber, "One-Pion Exchange in the $K^+ + p \rightarrow \bar{K}^* + N^*$ Reaction," in Proceedings of the Conference on Fundamental-Particle Resonances, Ohio University, Athens, Ohio (June 1963).
8. S. Goldhaber, W. Chinowsky, G. Goldhaber, and T. O' Halloran, Bull. Am. Phys. Soc. 8, 20 (1963); S. Goldhaber, "Meson Exchange in K^+-p Reaction," in Proceedings of the Conference on Fundamental Particle Resonances, Ohio University, Atens, Ohio (June 1963).
9. C. Baltay, J. Sandweiss, J. Sanford, H. Brown, M. Webster, and S. Yamamoto, "The Separated Beam at the AGS--Performance with Antiprotons and π^+ Mesons," in Proceedings of the 1962 Conference on Instrumentation for High Energy Physics, CERN, 1962, (North Holland Publishing Co., Amsterdam, Holland, 1962); J. Leitner, G. Moneti, and N. P. Samios, "Performance of the AGS Separated Beam with High Energy Kaons," in Proceedings of the 1962 Conference on Instrumentation for High Energy Physics, CERN, 1962 (North Holland Publishing Co., Amsterdam, Holland, 1962).
10. The PANG program developed by the Alvarez group at the Lawrence Radiation Laboratory was used for the reconstruction. A description of the program is given by W. Humphrey, Lawrence Radiation Laboratory Alvarez Group Memo 115, 1959 (unpublished). For a description of the kinematical fitting program see A. H. Rosenfeld

(ed.), Reference Manual for KICK IBM Program, Lawrence Radiation Laboratory Report UCRL-9099, May, 1961 (unpublished). A description of the EXAMIN system is given by D. Johnson, Lawrence Radiation Laboratory Alvarez Group Memo 271, March 1961 (unpublished).

11. B. P. Roe, D. Sinclair, J. L. Brown, D. A. Glaser, J. A. Kadyk, and G. H. Trilling, Phys. Rev. Letters 7, 346 (1961).
12. The density used for liquid hydrogen was 0.0623 g/ml. See Thomas Ferbel, Antiproton-proton Interactions at 3.25 BeV/c (Ph. D. Thesis), Yale University, 1963 (unpublished).
13. This is a weighted average of the values $\tau = (0.86 \pm 0.03) \times 10^{-10}$ sec [G. Alexander, S. P. Almeida, and F. S. Crawford, Jr., Phys. Rev. Letters 9, 69 (1962)] and $\tau = (0.90 \pm 0.05) \times 10^{-10}$ sec [A. F. Garfinkel, Nevis Cyclotron Laboratory Report Nevis-104, April 1962 (unpublished)].
14. M. H. Alston, L. W. Alvarez, P. Eberhard, M. L. Good, W. Graziano, H. K. Ticho, and S. G. Wojcicki, Phys. Rev. Letters 6, 300 (1961).
15. S. B. Treiman and C. N. Yang, Phys. Rev. Letters 8, 140 (1962).
16. L. Stodolsky and J. J. Sakurai, Phys. Rev. Letters 11, 90 (1963).
17. B. Kehoe, Phys. Rev. Letters 11, 93 (1963).
18. G. F. Chew and F. E. Low, Phys. Rev. 113, 1640 (1959).
19. E. Ferrari and F. Selleri, Nuovo Cimento 27, 1450 (1963).
20. S. Berman (Stanford University, Stanford, California), private communication.
21. F. Selleri, Phys. Letters 3, 76 (1962).
22. M. Gell-Mann and K. M. Watson, Ann. Rev. Nucl. Sci. 4, 219 (1954).
23. Phase space is similarly treated by A. Pinski, Nuovo Cimento 24, 719 (1963).
24. The normalization of the matrix element is given by J. M. Jauch and F. Rohrlich, The Theory of Photons and Electrons (Addison-Wesley Publishing Company, Inc., Reading, Massachusetts, 1955). Sec. 8-6. The evaluation of the spin sums is given in Appendix A 2-5.

25. J. J. Sakurai, "New Mesons and Resonances in Strong Interaction Physics-Theoretical, in Proceedings of the International School of Physics "Enrico Fermi," Villa Monastero, Varenna, Como, Italy (to be published).